Net radiative forcing and air quality responses to regional CO emission reductions

M. M. Fry[1], **M. D. Schwarzkopf**[2], **Z. Adelman**[1], **V. Naik**[3], **W. J. Collins**[4], and **J. J. West**[1]

[1]Department of Environmental Sciences and Engineering, University of North Carolina at Chapel Hill, Chapel Hill, North Carolina, USA
[2]NOAA Geophysical Fluid Dynamics Laboratory, Princeton, New Jersey, USA
[3]UCAR/NOAA Geophysical Fluid Dynamics Laboratory, Princeton, New Jersey, USA
[4]Department of Meteorology, University of Reading, Reading, UK

Correspondence to: J. J. West (jjwest@email.unc.edu)

Abstract. Carbon monoxide (CO) emissions influence global and regional air quality and global climate change by affecting atmospheric oxidants and secondary species. We simulate the influence of halving anthropogenic CO emissions globally and individually from 10 regions on surface and tropospheric ozone, methane, and aerosol concentrations using a global chemical transport model (MOZART-4 for the year 2005). Net radiative forcing (RF) is then estimated using the GFDL (Geophysical Fluid Dynamics Laboratory) standalone radiative transfer model. We estimate that halving global CO emissions decreases global annual average concentrations of surface ozone by 0.45 ppbv, tropospheric methane by 73 ppbv, and global annual net RF by 36.1 mW m^{-2}, nearly equal to the sum of changes from the 10 regional reductions. Global annual net RF per unit change in emissions and the 100 yr global warming potential (GWP$_{100}$) are estimated as -0.124 mW m^{-2} (Tg CO)$^{-1}$ and 1.34, respectively, for the global CO reduction, and ranging from -0.115 to -0.131 mW m^{-2} (Tg CO)$^{-1}$ and 1.26 to 1.44 across 10 regions, with the greatest sensitivities for regions in the tropics. The net RF distributions show widespread cooling corresponding to the O$_3$ and CH$_4$ decreases, and localized positive and negative net RFs due to changes in aerosols. The strongest annual net RF impacts occur within the tropics (28° S–28° N) followed by the northern midlatitudes (28° N–60° N), independent of reduction region, while the greatest changes in surface CO and ozone concentrations occur within the reduction region. Some regional reductions strongly influence the air quality in other regions, such as East Asia, which has an impact on US surface ozone that is 93 % of that from North America. Changes in the transport of CO and downwind ozone production clearly exceed the direct export of ozone from each reduction region. The small variation in CO GWPs among world regions suggests that future international climate agreements could adopt a globally uniform metric for CO with little error, or could use different GWPs for each continent. Doing so may increase the incentive to reduce CO through coordinated policies addressing climate and air quality.

1 Introduction

Carbon monoxide (CO) is emitted from the incomplete combustion of carbon fuels, and contributes indirectly to climate change through its influence on tropospheric ozone (O$_3$) and atmospheric oxidants (e.g., hydroxyl radical (OH), hydrogen peroxide (H$_2$O$_2$), and O$_3$), which in turn affect the abundance of methane (CH$_4$) and aerosols (Pham et al., 1995; Unger et al., 2006; Shindell et al., 2009). CO emission reductions impact both climate and air quality by increasing tropospheric OH concentrations, which lead to decreases in global CH$_4$ and thus, long-term O$_3$ (Prather et al., 1996; Wild et al., 2001; Fiore et al., 2002; Naik et al., 2005), as CH$_4$ is a longer-lived precursor to tropospheric O$_3$ (West et al., 2007, 2009a; Fiore et al., 2009). Here, we assess the net climate impact of reducing anthropogenic CO emissions globally and from 10 world regions individually, to inform future policies that may

address air quality and climate jointly. We omit reductions in co-emitted species (e.g., black carbon (BC), and organic carbon (OC)) that would be affected by measures to reduce CO emissions, to examine the sensitivity of air quality and RF to CO emissions alone, and to derive CO climate metrics. Future studies may model emission control measures that address multiple species (e.g., Shindell et al., 2012), or combine these results with those for co-emitted pollutants to determine the net effect of emission control measures.

Tropospheric O_3 and CH_4, both greenhouse gases, have contributed abundance-based anthropogenic radiative forcings (RF) of 0.35 (-0.1, $+0.3$) $W\,m^{-2}$ and $0.48 \pm 0.05\,W\,m^{-2}$, respectively, the largest greenhouse gas forcings behind CO_2 (Forster et al., 2007). CO and volatile organic compounds (VOC) emissions provide important contributions toward these forcings, estimated as $0.21 \pm 0.10\,W\,m^{-2}$ due to tropospheric O_3 and CH_4 changes (Shindell et al., 2005; Forster et al., 2007), and $0.25 \pm 0.04\,W\,m^{-2}$ (from 1750 to 2000) when the effects on sulfate and nitrate aerosols and CO_2 are included (Shindell et al., 2009).

In addition to being near-term climate forcers, products of CO reactions (O_3 and aerosols) are important air pollutants. CO emissions not only affect O_3 concentrations locally, but also intercontinentally (Akimoto, 2003; TF HTAP, 2010), given tropospheric ozone's mean lifetime of 22 days (Stevenson et al., 2006) and CO's lifetime of 1 to 3 months, both of which exceed typical intercontinental transport times (5 to 10 days) (Fiore et al., 2009; West et al., 2009a). Because of its lifetime, the transport of CO makes an important contribution to long-range O_3 (Heald et al., 2003). However, recent studies have identified large uncertainties in regional CO emissions inventories (Duncan et al., 2007), compared to satellite data (Heald et al., 2004; Pétron et al., 2004; Pfister et al., 2004, 2005; Kopacz et al., 2009), e.g., underestimating tropical biomass burning emissions and northern midlatitude seasonal variation in bottom-up inventories (Kopacz et al., 2010). CO emissions also affect atmospheric aerosols including sulfate (SO_4^{2-}) by influencing the oxidation of sulfur dioxide (SO_2) by OH in the gas phase, or by H_2O_2 or O_3 in the aqueous phase. OH increases from CO reductions lead to increased gas-phase SO_4^{2-} formation, and hence, climate cooling, while H_2O_2 and O_3 decreases lead to decreased aqueous-phase SO_4^{2-} formation (locally to intercontinentally) and climate warming (Unger et al., 2006; Leibensperger et al., 2011). In addition, CO influences the abundance of ammonium nitrate (NH_4NO_3) and secondary organic aerosols (SOA) via oxidant changes (Bauer et al., 2007; Hoyle et al., 2009).

For more than a decade, many have suggested that short-lived climate forcers and their precursors, like CO, be considered in international climate agreements, in addition to national air quality programs (Fuglestvedt et al., 1999; Rypdal et al., 2005, 2009; Naik et al., 2005; Fry et al., 2012), and it is among these short-lived climate forcers for which reduc-

ing emissions can slow the near-term rate of climate change (Jackson, 2009; Shindell et al., 2012). One reason why CO has not been included in a climate mitigation strategy is that its RF varies by region of emissions, given its relatively short lifetime in the troposphere (Berntsen et al., 2005). Global warming potentials (GWP) have been estimated for global CO emissions, with values ranging from 1.0 to 3.0 for a 100 yr time horizon (GWP_{100}) (Fuglestvedt et al., 1996; Johnson and Derwent, 1996; Daniel and Solomon, 1998; Collins et al., 2002), based on O_3 production and feedbacks on CH_4. Few studies have estimated GWPs for CO emissions from particular world regions. Berntsen et al. (2005) estimated GWPs for CO emissions from Europe and Southeast Asia, finding that the GWP for Asian CO emissions was 25 % higher than that for European emissions. Fry et al. (2012) also calculated CO GWP estimates for four world regions using an ensemble of global models, showing a small range (GWP_{20}: 4.6 ± 1.3 to 5.3 ± 1.2; GWP_{100}: 1.5 ± 0.4 to 1.7 ± 0.5) with coefficients of variation (CV = standard deviation/mean) of 0.065 for GWP_{20} and 0.059 for GWP_{100}, where the European reduction produced a lower GWP than North America, East Asia, and South Asia reductions. Further research on the sensitivity of net RF and CO GWPs to the region of CO emissions, including regions within the tropics and Southern Hemisphere (SH), may inform future policies that address climate change over the next 30 yr, in coordination with longer-term CO_2 mitigation (Daniel and Solomon, 1998; Shindell et al., 2012).

In this paper, we evaluate the effects of 50 % anthropogenic CO emission reductions from 10 regions individually, and globally, on stratospheric-adjusted net RF, tropospheric burdens (O_3, CH_4, and aerosols), and surface O_3 air quality to inform future coordinated actions addressing air quality and climate. We simulate the influence of CO emission reductions on tropospheric chemical composition using a global chemical transport model (CTM) and then apply a standalone radiative transfer model (RTM) to estimate the RF from changes in O_3, CH_4, and the direct effect of aerosols. We present the variability in CO RF and GWPs from 10 regions, while previous studies only evaluated CO emissions perturbations from a few regions (Berntsen et al., 2005; Fiore et al., 2009; TF HTAP, 2010; Fry et al., 2012). The global annually averaged net RF estimates given here are indicators of global mean surface temperature changes, but do not account for regional climate changes from spatially nonuniform forcings (Shindell et al., 2009).

2 Methods

2.1 Chemical transport modeling

Using the Model for OZone And Related chemical Tracers, version 4 (MOZART-4) (Emmons et al., 2010), we simulate anthropogenic CO emission reductions from 10 regions
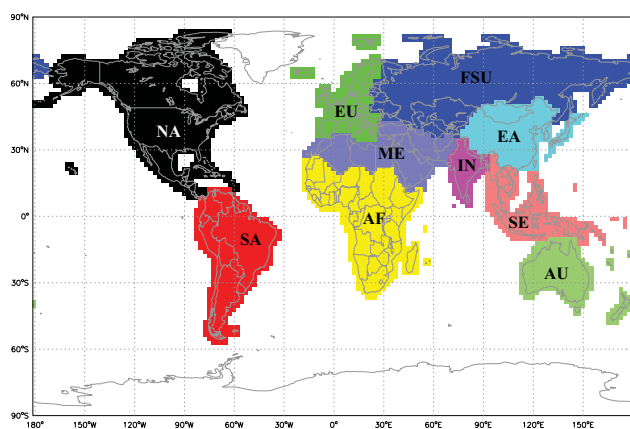
Fig. 1. Definition of 10 reduction regions.

(North America (NA), South America (SA), Europe (EU), Former Soviet Union (FSU), Africa (AF), India (IN), East Asia (EA), Southeast Asia (SE), Australia and New Zealand (AU), and Middle East and Northern Africa (ME)) (Fig. 1) and globally (sum of emissions from 10 regions only), relative to a base simulation. We use the Coupled Model Intercomparison Project phase 5 (CMIP5) Representative Concentration Pathway 8.5 (RCP8.5) emissions inventory for the year 2005 (Riahi et al., 2007, 2011) and global meteorology from the Goddard Earth Observing System Model, version 5 (GEOS-5) for the years 2004 to 2006 (Rienecker et al., 2008) as inputs to MOZART-4.

The RCP8.5 volatile organic compound (VOC) species are re-speciated to MOZART-4 VOC categories by matching like species. Monthly temporal variation is added to all emissions species from anthropogenic sources, in each grid cell, by scaling to the monthly profile of emission species in the REanalysis of the TROpospheric chemical composition over the past 40 yr (RETRO) global emissions dataset (Schultz et al., 2007), while shipping, aircraft, and biomass burning emissions already have monthly temporal variation. Biogenic emissions of isoprene and monoterpenes are calculated online in MOZART-4 using the Model of Emissions of Gases and Aerosols from Nature (MEGAN) (Guenther et al., 2006), based on the methods of Pfister et al. (2008); global annual isoprene and monoterpene emissions are $738\,\mathrm{Tg\,yr^{-1}}$ and $107\,\mathrm{Tg\,yr^{-1}}$. All other natural emissions are taken from the Precursors of Ozone and their Effects in the Troposphere (POET) emissions inventory for the year 2000 (Olivier et al., 2003; Granier et al., 2005; Emmons et al., 2010). The global annual mean lightning NO_x and soil NO_x emissions (for 2005) are estimated as $2.4\,\mathrm{Tg\,N\,yr^{-1}}$ and $8.0\,\mathrm{Tg\,N\,yr^{-1}}$, respectively, which are within the range of other modeling studies (Schumann and Huntrieser, 2007; Hudman et al., 2012).

The global and regional reduction simulations are run from 1 July 2004 through 31 December 2005 at $1.9° \times 2.5°$ (lati-

tude $\times$ longitude) horizontal resolution and 56 vertical levels. The base simulation is run through 31 December 2006 to allow further comparisons with observations. Although the perturbation simulations are 1.5 yr in length, we account for the influence of CO emissions on CH_4 (via OH), and thus long-term changes in O_3 on the decadal timescale of CH_4 perturbation lifetime, using methods from previous studies (Prather et al., 2001; West et al., 2007; Fiore et al., 2009; Fry et al., 2012). We set global CH_4 to a uniform mixing ratio in the base and perturbation simulations of 1783 parts per billion by volume (ppbv) (WMO, 2006). We then simulate an additional CH_4 control simulation, which reduces global CH_4 by 20 % to 1426.4 ppbv. Using the results from the base and CH_4 control simulations, we estimate CH_4 lifetime against loss by tropospheric OH (τ_{OH}, 11.24 yr), total CH_4 lifetime based on τ_{OH} and CH_4 loss to soils and the stratosphere (τ_{total}, 9.66 yr), and methane's feedback factor (F, 1.29) by the methods of Prather et al. (2001) and more recently, Stevenson et al. (2013), finding that our τ_{OH} agrees with a recent estimate of τ_{OH} based on observations (11.2 ± 1.3 yr) (Prather et al., 2012), and is within the range of other models: 8.2 to 11.7 yr (Stevenson et al., 2006), 10.2 ± 1.7 yr (Fiore et al., 2009), and 9.8 ± 1.6 yr (Voulgarakis et al., 2013). Using the offline formulation of West et al. (2007) and our estimated parameters (τ_{OH}, τ_{total}, and F), we estimate the steady-state tropospheric CH_4 change for each perturbation. We then calculate long-term O_3 responses by scaling the change in O_3 from the CH_4 control simulation (CH_4 control simulation minus base) in each grid cell by the ratio of global CH_4 burden change calculated for each perturbation to that of the CH_4 control simulation. Long-term O_3 responses are added to the short-term O_3 responses simulated directly for each CO emission reduction (described below) to yield O_3 concentrations at steady state (West et al., 2007; Fiore et al., 2009; Fry et al., 2012).

Because MOZART-4 does not have complete stratospheric chemistry (Emmons et al., 2010), three-dimensional monthly mean stratospheric O_3 concentrations from the AC&C/SPARC (Stratospheric Processes And their Role in Climate) O_3 database prepared for CMIP5 (available at: http://pcmdi-cmip.llnl.gov/cmip5/forcing.html) (Cionni et al., 2011) are merged with the calculated steady-state (short-term + long-term) tropospheric O_3 concentrations for each simulation including the base case. Søvde et al. (2011) estimated that ~15 % of the RF of O_3 precursors is due to lower stratosphere O_3 changes, using a single model with both standard and updated chemistry. Since we do not account for lower stratospheric O_3 changes, our RF estimates may underestimate the full effect of CO emissions.

MOZART-4 simulates the tropospheric aerosols SO_4^{2-}, BC, OC, primary and secondary organics, NH_4NO_3, and sea salt aerosols (Lamarque et al., 2005; Emmons et al., 2010). Here we quantify the changes in SO_4^{2-}, NH_4NO_3, and SOA, as these aerosols are most directly influenced by anthropogenic CO emissions via changes in oxidants.
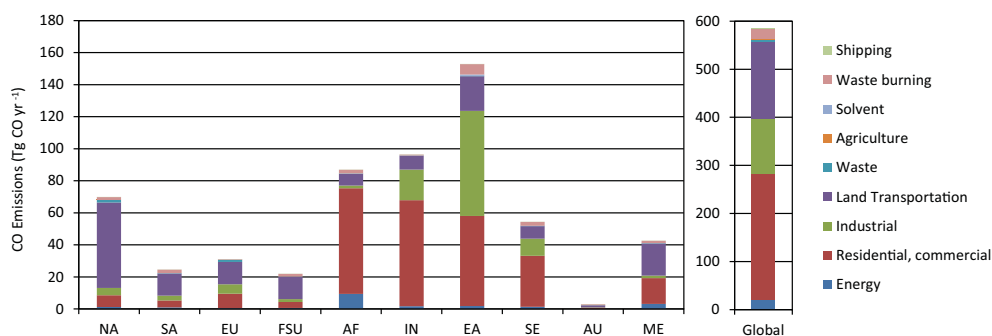
Fig. 2. Annual average anthropogenic CO emissions (Tg CO yr^{-1}) by region and sector for the base simulation, from the RCP8.5 emissions inventory for the year 2005.

SO_4^{2-} aerosols in MOZART-4 are produced from SO_2 and dimethylsulfide (DMS) emissions through gas and aqueous-phase oxidation (Barth et al., 2000), while NH_4NO_3 aerosols are calculated from the oxidation of nitrogen oxides (NO_x) to nitric acid (HNO_3), and subsequent reaction with NH_3 emissions (Metzger et al., 2002). SOA is formed through the gas-phase oxidation of monoterpenes by OH, O_3, and nitrate (NO_3), and the gas-phase oxidation of toluene by OH (Chung and Seinfeld, 2002).

Each perturbation simulation reduces anthropogenic CO emissions by 50 % in one region (or globally), while leaving all other emissions unchanged. Figure 2 shows the total anthropogenic CO emissions by region and sector for the base simulation. Anthropogenic CO emissions include all source categories in Fig. 2, but exclude biomass burning (except for the agriculture and waste burning categories), such as forest fires and grassland fires, which are also large sources of CO. We exclude biomass burning as actions to address biomass burning differ from the other sectors addressed here, and would reduce a suite of emissions simultaneously (Naik et al., 2007). Using the global, three-dimensional results from each perturbation, global and regional changes in air quality (O_3 and aerosols) at the surface (within the first vertical level) and across the troposphere (region with O_3 levels less than 150 ppbv) are quantified, relative to the base simulation, including the influence of each regional reduction on O_3 long-range transport.

2.2 MOZART-4 evaluation

Previous MOZART-4 simulations, with comparable model formulations but different inputs, have reproduced O_3 and CO observations well (e.g., Pfister et al., 2005, 2006, 2008; Lapina et al., 2006; Horowitz et al., 2007; and Emmons et al., 2010). Table 1 summarizes the total anthropogenic CO emissions and annual average surface O_3, SO_4^{2-}, and CO concentrations regionally and globally for the base simulation. The base simulation produces an average bias of 4.5 ppbv O_3 across all sites compared to the Clean Air Status and Trends Network (CASTNET) (Fig. S1), and 0.8 ppbv O_3

compared to the European Monitoring and Evaluation Programme (EMEP) network (Fig. S2). MOZART-4 performs the least well during the summer months (June to August) in the US, with biases of nearly 20 ppbv in the Great Lakes, northeast US, and southeast US regions. Simulated annual average surface SO_4^{2-} concentrations are mostly within a factor of two of observations from the Interagency Monitoring of Protected Visual Environments (IMPROVE) and EMEP monitoring networks for 2005 (Fig. S3). The base simulated monthly mean surface CO concentrations also generally agree with the seasonal cycle of NOAA CMDL (Climate Monitoring and Diagnostics Laboratory) surface CO measurements, but overestimate CMDL measurements in the SH (Fig. S4), as was also found by Emmons et al. (2010).

Simulated monthly 2005 and 2006 vertical O_3 profiles are comparable to 1995 to 2009 monthly mean and median ozonesonde climatology (Tilmes et al., 2012) (Fig. S5), with the greatest agreement at 800 and 500 millibar (mb) altitudes (Fig. S6). Larger differences exist between the base simulated O_3 and ozonesonde climatology at 200 mb, which may reflect the model's upper boundary conditions and constraints (Emmons et al., 2010).

Our base 2005 simulated OH burdens are lower than Spivakovsky et al. (2000), but fairly comparable to those of Lawrence (1996), Lawrence et al. (1999), von Kuhlmann (2001), and Emmons et al. (2010) (Table S1). Low modeled OH concentrations may contribute in part to the surface CO overestimates of CMDL measurements in the SH. The percentage loss of tropospheric CH_4 by reaction with OH in the base simulation is comparable to Fiore et al. (2008) (Table S2), yet slightly lower in the lower troposphere (surface to 750 hPa), and slightly higher in the mid- and upper troposphere (750 to 250 hPa).

2.3 Radiative transfer modeling

The NOAA Geophysical Fluid Dynamics Laboratory (GFDL) RTM is used to estimate the stratospheric-adjusted net RF due to changes in tropospheric steady-state O_3, CH_4, and SO_4^{2-} aerosols (direct effect). The GFDL RTM

Table 1. For the base simulation, total anthropogenic CO emissions by region, and regional (or global) annual average area-weighted surface O_3, SO_4^{2-}, and CO concentrations.

Reduction region	Total anthropogenic CO emissions (Tg yr^{-1})	Annual average surface O_3 (ppbv)	Annual average surface SO_4^{2-} ($\mu g\,m^{-3}$)	Annual average surface CO (ppbv)
NA	70.0	35.3	1.6	151.0
SA	24.5	24.8	0.7	147.4
EU	31.2	36.5	3.0	166.0
FSU	21.9	33.2	1.4	166.3
AF	86.9	30.0	0.9	172.9
IN	96.4	41.2	2.9	279.4
EA	152.9	42.4	4.3	235.0
SE	54.3	28.1	1.6	174.5
AU	2.9	22.8	0.5	101.9
ME	42.6	40.4	2.5	147.5
Global	584.7	26.2	1.0	122.7

Table 2. Source–receptor matrix of annual average surface CO concentration changes (ppbv), for the regional reduction simulations, with the United States (US) also defined as a receptor in addition to the 10 regions. The largest changes for each source reduction region are in bold.

Source	Receptor										
	NA	SA	EU	FSU	AF	IN	EA	SE	AU	ME	US
NA	−12.5	−0.69	−4.56	−4.07	−1.34	−1.75	−3.27	−1.17	−0.32	−3.36	**−19.3**
SA	−0.19	**−3.81**	−0.13	−0.13	−0.56	−0.32	−0.17	−0.45	−0.83	−0.18	−0.15
EU	−2.32	−0.31	**−18.3**	−4.96	−0.98	−0.85	−2.56	−0.63	−0.13	−3.90	−2.16
FSU	−2.05	−0.18	−3.66	**−9.70**	−0.47	−0.69	−2.96	−0.49	−0.08	−2.03	−1.88
AF	−1.05	−2.47	−0.87	−0.87	**−10.2**	−1.84	−1.11	−1.47	−1.58	−1.42	−0.95
IN	−1.93	−1.03	−1.82	−2.00	−2.21	**−75.5**	−4.23	−3.50	−0.57	−2.76	−1.97
EA	−7.08	−1.29	−6.53	−7.68	−2.36	−4.79	**−50.0**	−8.36	−0.73	−5.08	−7.52
SE	−0.82	−0.72	−0.74	−0.73	−0.90	−1.90	−1.48	**−8.96**	−0.73	−0.83	−0.83
AU	−0.01	−0.11	−0.01	−0.01	−0.07	−0.04	−0.01	−0.10	**−0.81**	−0.02	−0.01
ME	−1.65	−0.49	−2.33	−2.95	−1.69	−5.91	−2.51	−0.94	−0.22	**−13.7**	−1.66

is a module of the GFDL coupled atmosphere-ocean model (AM2) and simulates solar and infrared radiative transfer (GFDL GAMDT, 2004; Naik et al., 2005, 2007). This RTM has been applied in studies of long-lived greenhouse gases (Schwarzkopf and Ramaswamy, 1999) and short-lived forcing agents (Naik et al., 2005, 2007; West et al., 2007; Fiore et al., 2008; Saikawa et al., 2009; Fry et al., 2012). Here the RTM is employed as in Fry et al. (2012) at $144 \times 90 \times 24$ levels, and with updated well-mixed greenhouse gas concentrations including CO_2 and nitrous oxide (N_2O) (Meinshausen et al., 2011) and CMIP5 solar forcing data (http://www.geo.fu-berlin.de/en/met/ag/strat/forschung/SOLARIS/Input_data/CMIP5_solar_irradiance.html). The RTM simulations do not include the indirect effects of aerosols on clouds or the internal mixing of aerosols. Aerosol indirect effects are highly uncertain, and may account for considerable RF contributions beyond the direct effect of aerosols (Forster et al., 2007). Changes in the RF

contributions from nitrate aerosols, stratospheric O_3, water vapor, the carbon cycle via O_3 and nitrogen deposition, and CO_2 (from changes in CH_4 and CO oxidation) are also excluded. CO oxidizes to CO_2 in the atmosphere, with a minor influence on the net RF of CO (Shindell et al., 2009). Since this carbon is likely already accounted for in inventories of CO_2, we do not estimate CO_2 forcing here (Daniel and Solomon, 1998).

Tropospheric O_3, CH_4, SO_4^{2-}, BC, and OC concentrations from the MOZART-4 base and perturbed simulations are used as inputs to the RTM simulations, along with meteorological fields from GFDL's atmosphere model (AM2) and land model (LM2), sampled one day per month at mid-month for the year 2005, to represent monthly mean conditions (Naik et al., 2005). BC and OC concentrations are not evaluated further as changes in these species between the base and perturbed simulations are negligible, but we include them as inputs to the RTM simulations. The RTM currently
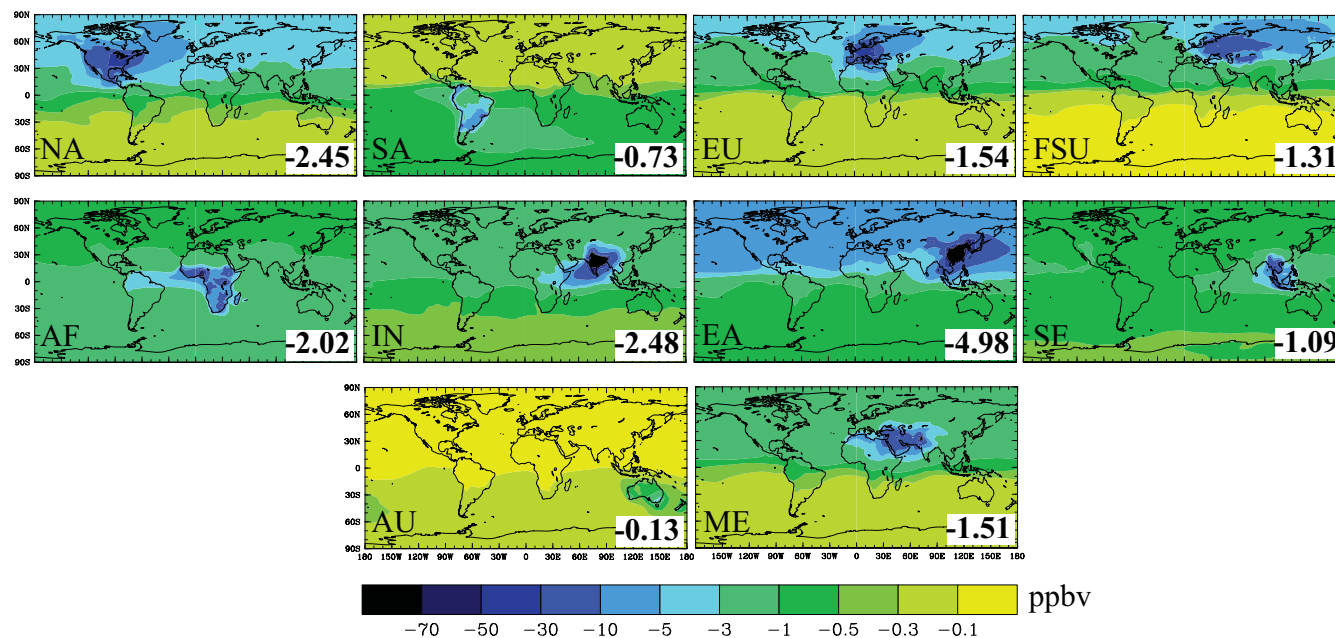
Fig. 3. Global distribution of annual average surface CO concentration changes (ppbv) for each of the regional reduction simulations relative to the base. The global annual average surface CO concentration changes (ppbv) for each simulation are noted in the lower right of each panel.

does not calculate the RF of SOA and NH_4NO_3 aerosols. The net RF is calculated as the difference between the perturbed and base cases' simulated monthly mean net radiation fluxes (net shortwave minus net longwave), in each grid cell and month, at the tropopause after allowing stratospheric temperatures to readjust to radiative equilibrium (Naik et al., 2007; Saikawa et al., 2009; Fry et al., 2012).

3 Global and regional air quality responses

3.1 Surface CO concentrations

We first analyze the magnitude and distribution of annual average surface CO concentrations for each 50 % reduction in anthropogenic CO emissions, relative to the base. Figure 3 shows that the largest decreases in surface CO occur within each reduction region, with lesser decreases intercontinentally. The foreign region that most influences the US is EA, which contributes 39 % of the change in US surface CO that results from the NA reduction (Table 2). Responses normalized by emission change are listed in Table S3. Given that modeled OH concentrations are lower than a previous study (Spivakovsky et al., 2000), simulated surface CO concentrations may be slightly overestimated, such as in the SH when compared to CMDL measurements.

3.2 Responses of methane and ozone

3.2.1 Tropospheric methane

Changes in global tropospheric steady-state CH_4 abundance for each perturbation relative to the base are calculated using the tropospheric CH_4 loss flux diagnosed from the model (West et al., 2007; Fiore et al., 2009; Fry et al., 2012) (Table 3). The EA reduction produces the greatest change in global CH_4 (−19.4 ppbv), followed by IN (−11.5 ppbv) and AF (−10.9 ppbv) reductions. Upon normalizing by the change in CO emissions, global CH_4 varies little among regions (CV = 0.054), suggesting that the sensitivity of global CH_4 to CO emissions is nearly independent of emission region (Fig. S7, Table S9). Fry et al. (2012) also found that CH_4 sensitivity to CO emission changes varies little (0.22 to 0.24 ppbv CH_4 (Tg CO)$^{-1}$), in contrast to the more regionally-variable effects of NO_x and NMVOC (non-methane volatile organic compound) emissions on CH_4.

3.2.2 Surface and tropospheric ozone

Global CH_4 changes are used to calculate long-term tropospheric O_3 changes, which vary little among regions, that are then added to short-term changes to give steady-state O_3 responses (Table 4). Steady-state global O_3 changes are 40 to 83 % greater than short-term changes, suggesting that the long-term influence of CO via CH_4 is relevant for air quality (West et al., 2007). Both short-term and steady-state global surface O_3 responses are approximately proportional to the

Table 3. For the global and regional reduction simulations relative to the base, global annual mean burden changes in tropospheric and upper tropospheric (UT) steady-state O_3, tropospheric CH_4, SO_4^{2-}, NH_4NO_3, and SOA. The total global annual average tropospheric O_3 (at steady state), SO_4^{2-}, NH_4NO_3, and SOA burdens in the base simulation are 352 Tg O_3, 1788 Gg SO_4^{2-}, 457 Gg NH_4NO_3, and 237 Gg SOA.

Reduction region	ΔO_3 (Tg)	ΔUT O_3 (Tg)	ΔCH_4 (ppbv)	ΔSO_4^{2-} (Gg)	ΔNH_4NO_3 (Gg)	ΔSOA (Gg)
NA	−0.64	−0.37	−9.1	−0.54	0.24	−0.11
SA	−0.21	−0.14	−3.2	−0.05	−0.003	−0.02
EU	−0.27	−0.15	−4.1	−0.37	0.19	−0.07
FSU	−0.19	−0.11	−2.9	−0.22	0.12	−0.05
AF	−0.80	−0.51	−10.9	0.03	−0.09	−0.06
IN	−0.93	−0.61	−11.5	0.48	−0.29	−0.17
EA	−1.38	−0.84	−19.4	−1.25	0.22	−0.43
SE	−0.56	−0.38	−6.6	−0.11	−0.04	−0.12
AU	−0.02	−0.01	−0.4	−0.01	0.001	−0.001
ME	−0.38	−0.23	−5.6	0.37	0.003	−0.09
Global	−5.39	−3.35	−73.0	−1.82	0.39	−1.11
CH_4 control	−8.76	−2.30	−356.6	−3.05	0.78	0.26

Table 4. For the global and regional reduction simulations, global annual mean changes in short-term surface O_3, steady-state surface O_3, steady-state surface O_3 per unit change in CO emissions, and long-term surface O_3 per unit change in CO emissions.

Reduction region	Δ Short-term surface O_3 (pptv)	Δ Steady-state surface O_3 (pptv)	Δ Steady-state surface O_3 per Tg CO emissions (pptv $(Tg\,CO\,yr^{-1})^{-1}$)	Δ Long-term surface O_3 per Tg CO emissions (pptv $(Tg\,CO\,yr^{-1})^{-1}$)
NA	−42.8	−63.0	−1.8	−0.58
SA	−8.7	−15.9	−1.3	−0.59
EU	−22.1	−31.2	−2.0	−0.58
FSU	−16.0	−22.4	−2.1	−0.58
AF	−31.3	−55.4	−1.3	−0.55
IN	−40.8	−66.4	−1.4	−0.53
EA	−77.8	−120.8	−1.6	−0.56
SE	−19.9	−34.5	−1.3	−0.54
AU	−1.2	−2.2	−1.5	−0.68
ME	−24.1	−36.5	−1.7	−0.58
Global	−287.8	−450.1	−1.5	−0.56

level of CO emissions change (Fig. 4). Values in Table 4 could be scaled to other emissions changes, allowing long-term effects to be included in future global or regional modeling exercises (e.g., West et al., 2009b for NO_x).

Surface O_3 responses are greatest within the hemisphere of reduction; since inter-hemispheric transport takes about 1 yr, little mixing occurs across hemispheres (Jacob, 1999; West et al., 2009a). The long-term O_3 component (via CH_4), however, impacts air quality globally. The distributions of steady-state surface O_3 changes are shown in Fig. 5, and are quantified as annual average changes within all 10 regions and the US (Table 5). The greatest steady-state surface O_3 decreases occur within the reduction region, with smaller decreases hemispherically, except for the AU reduction, which has little effect (< 2.1 pptv) on foreign regions (Table 5). Similar trends are seen in regional steady-state surface O_3 responses normalized per unit change in CO emissions (Table S4).

The sum of global annual mean steady-state surface O_3 changes from the 10 regional reductions (-448 pptv) is nearly equivalent to that of the global CO reduction (-450 pptv). However, steady-state surface O_3 (normalized per unit change in CO emissions) is most sensitive to FSU and EU reductions (-2.1 and -2.0 pptv/Tg CO yr^{-1}, respectively) (Table 4). The largest CO emitters (EA, IN, AF, and NA) (Table 1) produce the greatest impacts within the reduction region or between regions. EA is the foreign region that most influences the US, with an influence on surface O_3 that is nearly as large (93 %) as the influence from NA CO emissions. Fiore et al. (2009) also found that East Asia CO emissions can influence surface O_3 in North America by as much as 50 % of the response from domestic emissions. Reducing NA CO emissions strongly impacts EU and ME surface O_3, with an influence that is 77 and 75 %, respectively, of domestic impacts. In some cases, foreign CO emission reductions

Table 5. Source–receptor matrix of annual average steady-state changes in surface O_3 concentrations (pptv), for the regional reduction simulations, with the United States (US) also defined as a receptor in addition to the 10 regions. The largest changes for each source reduction region are in bold.

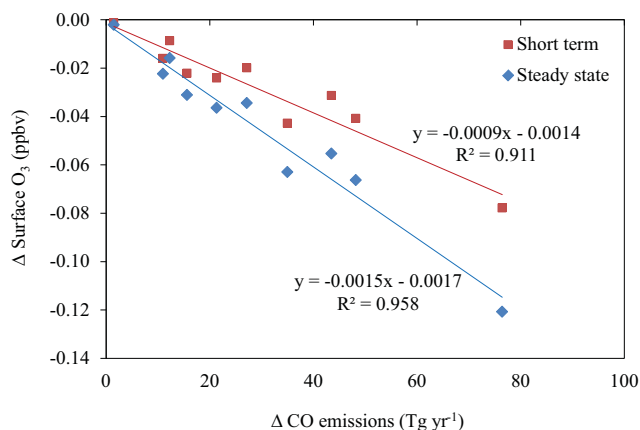|	Receptor										
Source	NA	SA	EU	FSU	AF	IN	EA	SE	AU	ME	US
NA	−178.2	−26.0	−131.1	−97.3	−46.8	−71.5	−102.4	−35.1	−20.7	−119.6	**−253.3**
SA	−14.4	**−25.3**	−14.2	−11.9	−16.4	−17.5	−15.6	−12.9	−15.2	−17.1	−15.4
EU	−48.4	−11.3	**−170.8**	−68.9	−24.7	−32.9	−57.9	−16.4	−9.1	−91.5	−56.0
FSU	−36.9	−7.6	−58.3	**−75.1**	−14.5	−25.8	−53.3	−12.1	−6.3	−50.9	−43.5
AF	−59.8	−52.1	−59.6	−49.9	**−97.2**	−77.2	−66.4	−46.0	−41.5	−77.7	−64.1
IN	−85.0	−37.6	−89.0	−76.8	−66.9	**−454.6**	−129.2	−67.2	−30.7	−114.5	−96.0
EA	−197.0	−53.4	−209.2	−178.2	−90.5	−158.6	**−437.7**	−118.9	−45.7	−202.0	−235.7
SE	−41.5	−24.3	−42.6	−35.6	−34.5	−57.0	−52.3	**−57.9**	−24.0	−50.0	−46.4
AU	−1.6	−1.9	−1.6	−1.4	−1.9	−2.1	−1.8	−2.0	**−4.8**	−2.0	−1.7
ME	−49.7	−17.1	−63.4	−59.0	−38.4	−105.9	−69.1	−25.0	−13.4	**−159.3**	−57.5

Fig. 4. Short-term and steady-state surface ozone changes as a function of CO emissions change for each of the regional reductions relative to the base.

have a greater impact on O_3 than a region's own domestic reduction, such as EA which reduces surface O_3 in EU by 22 % more than the EU reduction (Table 5). As in Fiore et al. (2009), for NH sources and receptors, the greatest transport and intercontinental influences of each region on other regions are mainly from March to June (Fig. S10).

The distributions of steady-state tropospheric total column O_3 changes (Fig. 6) are similar to surface O_3 responses (Fig. 5), yet more widespread hemispherically to globally. The troposphere is defined for O_3 less than 150 ppbv, and the upper troposphere (UT) from 500 hPa to the tropopause. We distinguish between full troposphere and UT O_3 burdens, since O_3 in the UT has a higher RF efficiency per molecule (Lacis et al., 1990; Wang et al., 1993; Forster and Shine, 1997). The EA reduction has the strongest impact on total column O_3 across the NH, while the AU CO reduction has the least impact on total column O_3 globally. Tropospheric total column O_3 changes are less than 2 % in all locations,

for each perturbation (Fig. S11). Normalized global annual mean full and UT steady-state O_3 burden changes (Table S5) are greatest for SE, IN, and AF reductions, due to the stronger photochemistry and more active vertical convection in the tropics.

3.3 Response of aerosols

Tropospheric annual mean burden changes in SO_4^{2-}, NH_4NO_3, and SOA are presented in Table 3. The IN, ME, and AF reductions increase the global SO_4^{2-} burden, while all other perturbations decrease global SO_4^{2-}. Global NH_4NO_3 burden also increases and decreases across the regional perturbations, but the global SOA burden decreases in all cases. The sums of global SO_4^{2-}, NH_4NO_3, and SOA burden changes for all 10 regional reductions are 0–8 % less than those of the global CO reduction, suggesting some dependence on regional conditions and chemistry. Increases in OH are expected to increase the global annual average SO_4^{2-}, NH_4NO_3, and SOA burdens, while decreases in O_3 (and H_2O_2 for SO_2 oxidation) are expected to decrease the global annual average SO_4^{2-} and SOA burdens.

Most regional perturbations show stronger increases in tropospheric OH within the source region, and smaller, widespread increases in the tropics (30° S to 30° N) (Fig. S12). Tropospheric total column H_2O_2 changes are opposite in sign, with the greatest decreases within the reduction region and extending longitudinally (Fig. S13).

In Fig. 7, annual average tropospheric total column SO_4^{2-} changes result from several SO_2 oxidation pathways, where CO's lifetime is long enough that the resulting SO_4^{2-} patterns are fairly independent of reduction region. In the northern midlatitudes, SO_4^{2-} decreases likely relate to the prevalence of clouds and decreased aqueous-phase SO_2 oxidation (in clouds) by O_3 and H_2O_2. Near the equator and in drier regions (i.e., near ME and AF), gas-phase SO_2 oxidation by OH dominates, leading to increases in SO_4^{2-}. The greatest
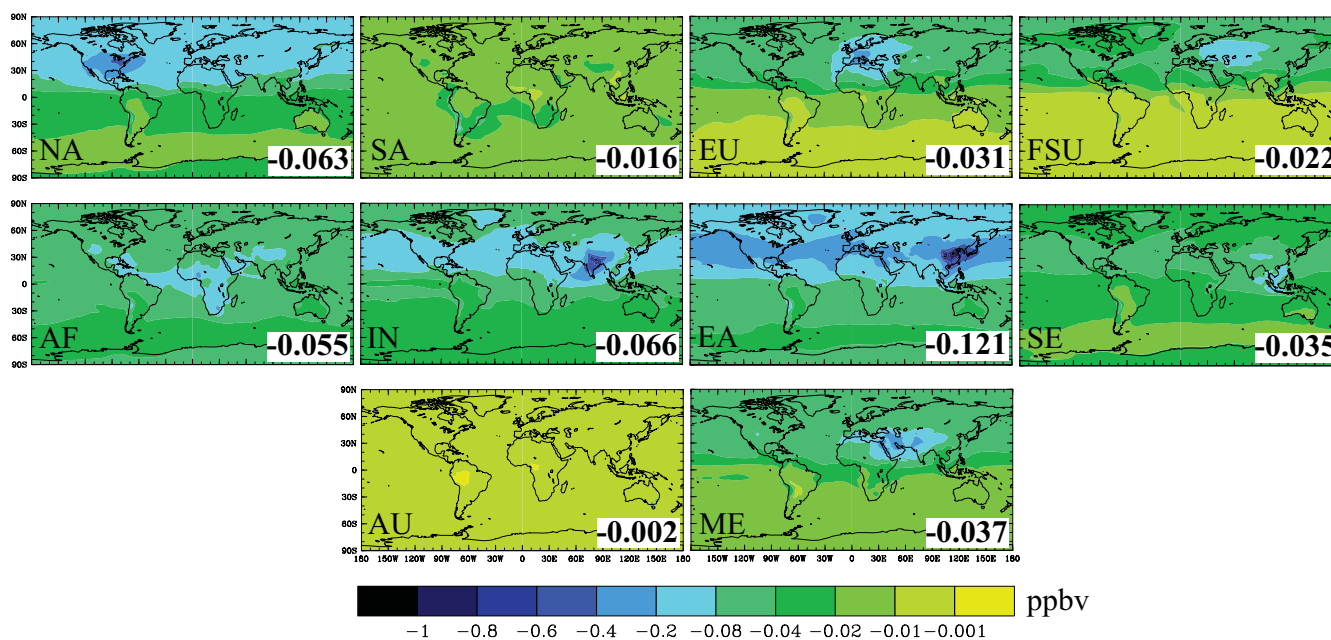
Fig. 5. Global distribution of annual average steady-state surface O_3 concentration changes (ppbv) for each of the regional reduction simulations relative to the base. The global annual average steady-state surface O_3 concentration changes (ppbv) for each simulation are noted in the lower right of each panel.

Table 6. For each regional reduction, changes in global annual average (short-term) tropospheric CO burden (B_{CO}), and B_{CO} per unit change in CO emissions (E_{CO}). Also shown are CO lifetime calculated as $\Delta B_{CO}/(\Delta E_{CO} + \Delta P_{CO})$, the fractions of B_{CO} change outside each reduction region and in the UT, and the changes in net CO export (X_{CO}) from the reduction region, global CO production (P_{CO}), and P_{CO} outside the reduction region. The total global annual average CO burden in the base simulation is 462.6 Tg CO.

Reduction region	ΔB_{CO} short-term (Tg CO)	$\Delta B_{CO}/\Delta E_{CO}$ (days)	CO Lifetime (days)	Fraction of ΔB_{CO} outside region	Fraction of ΔB_{CO} in UT	ΔX_{CO} from region (Tg yr^{-1})	ΔP_{CO} global (Tg yr^{-1})	ΔP_{CO} outside region (Tg yr^{-1})
NA	−6.7	70.3	78.2	0.82	0.37	−27.4	3.5	2.7
SA	−2.5	74.0	82.2	0.88	0.41	−10.4	1.2	1.0
EU	−3.4	79.3	88.2	0.92	0.30	−13.7	1.6	1.4
FSU	−2.5	83.7	93.1	0.79	0.29	−9.1	1.1	0.95
AF	−7.9	66.2	73.4	0.83	0.44	−33.6	4.3	3.3
IN	−8.0	60.5	66.7	0.92	0.45	−40.2	4.5	3.8
EA	−14.7	70.1	77.7	0.90	0.39	−64.6	7.5	6.5
SE	−4.9	66.4	73.4	0.89	0.50	−23.4	2.6	2.2
AU	−0.3	84.2	94.1	0.92	0.35	−1.3	0.2	0.14
ME	−4.0	68.2	75.8	0.90	0.36	−17.8	2.1	1.8

total column SO_4^{2-} percentage decreases (i.e., for NA, EU, and EA reductions) and greatest SO_4^{2-} percentage increases (i.e., for AF, IN, EA, and ME reductions) over the reduction region are 2 % or less. Intercontinental to hemispheric effects are generally 0.1 % or less, for all regional reductions (Fig. S14). Global annual average tropospheric NH_4NO_3 and SOA changes are likewise small: −21 and 61 %, respectively, of tropospheric SO_4^{2-} changes, for the global CO reduction. Our regional annual average surface $PM_{2.5}$ changes (0.059 µg m^{-3} or less) are only slightly smaller than those

estimated by Leibensperger et al. (2011) (∼0.1 µg m^{-3} from Asian NO_x and CO on northern Europe and eastern China, and ∼0.25 µg m^{-3} from US NO_x and CO on northern Europe and eastern China) who zeroed-out anthropogenic emissions, while we halve them here. CO generally does not have a strong influence on $PM_{2.5}$ air quality in our simulations.
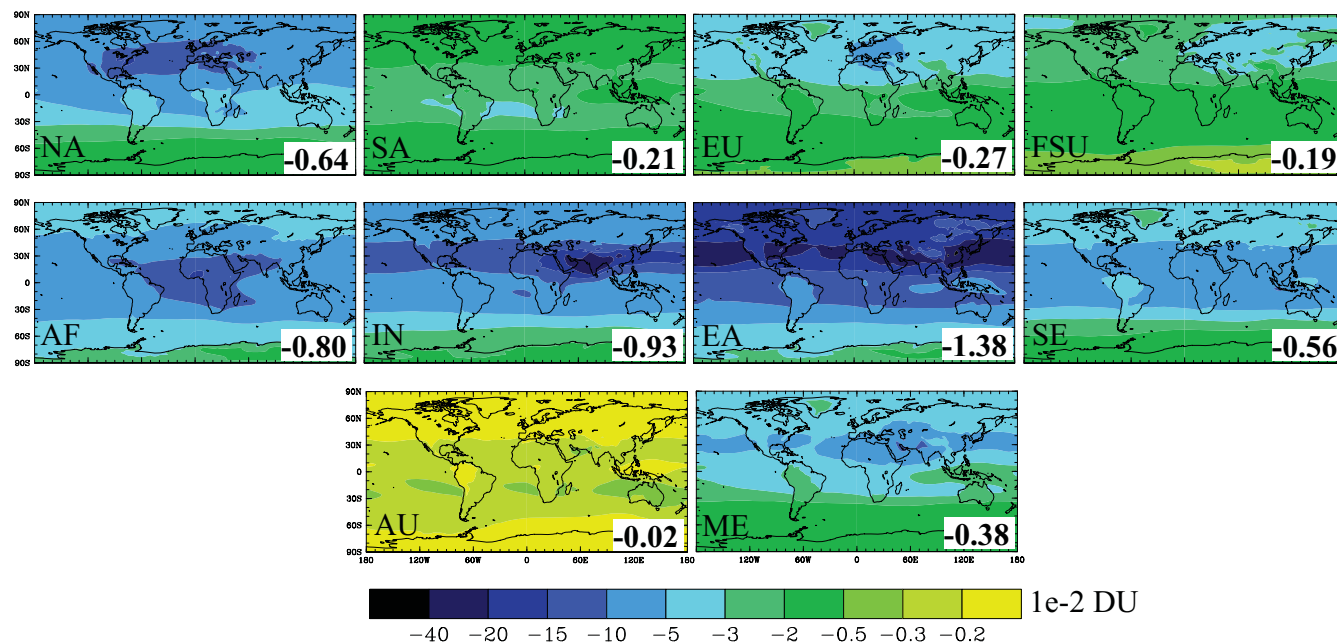
Fig. 6. Global distribution of annual average changes in tropospheric total column O_3 at steady state (1×10^{-2} DU) for each of the regional reduction simulations relative to the base. The global annual average steady-state tropospheric O_3 changes (1×10^{-2} DU) for each simulation are noted in the lower right of each panel.
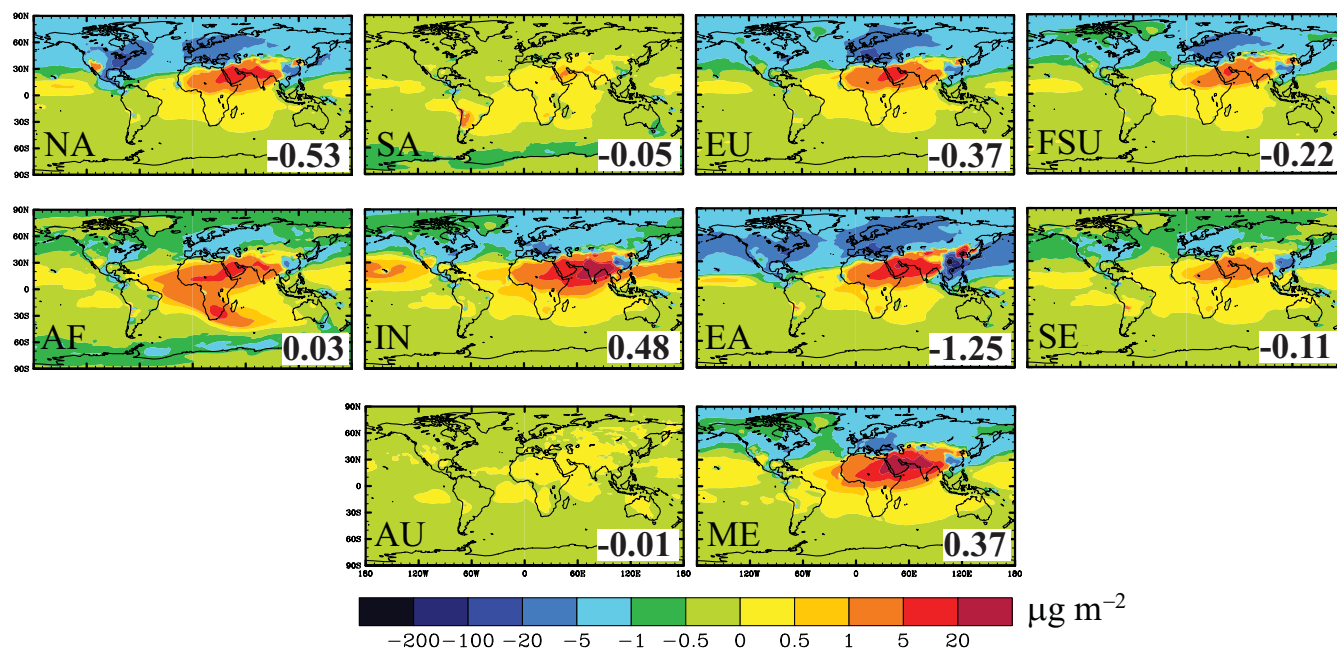

Fig. 7. Global distribution of annual average changes in tropospheric total column SO_4^{2-} ($\mu g\,m^{-2}$) for each of the regional reduction simulations relative to the base. The global annual average tropospheric SO_4^{2-} changes ($\mu g\,m^{-2}$) for each simulation are noted in the lower right of each panel.

4   Changes in production and export of CO and ozone

SA, EU, FSU, and AU reductions produce the greatest changes in global CO burden per unit change in CO emis-sions, and also result in the longest CO lifetimes (82 to 94 days) (Table 6, Table S9). More than 79 % of CO burden changes occur outside of the reduction region for all per-turbations, and between 41 and 50 % of CO burden changes

take place in the UT for SE, SA, AF, and IN reductions, consistent with the regions that have the greatest impact on O_3 production in the UT (Table 7). We find decreases in CO export from the reduction region in all cases, and increases in global CO production. These increases in CO production ($\sim 2\%$ for the global CO reduction) result from tropospheric OH increases that cause faster oxidation of CH_4 and NMVOCs (Shindell et al., 2006). However, the global CO loss frequency (or inverse lifetime) (Prather et al., 2012) increases by $\sim 3.4\%$ for the global CO reduction, indicating that as CO is reduced, increases in OH lead to further CO loss. Therefore in this study, the CO perturbation lifetime ($\Delta B_{CO}/\Delta E_{CO}$) is slightly greater than the CO atmospheric lifetime ($B_{CO}/(E_{COanthro} + E_{COnatural} + P_{CO})$) (feedback factor of ~ 1.06), which suggests that perturbing CO emissions can have an overall amplifying effect. Although we do not account for the long-term effects on CH_4 directly in our 1.5 yr simulations, these can be calculated offline from the changes in CH_4 lifetime as was done for O_3. Global CH_4 decreases also lead to decreases in CO production at steady state, and furthermore, increases in OH that cause increases in CO loss and production. These are summarized in Table S9. The long-term changes further amplify the CO signal leading to a total increase in CO loss frequency of $\sim 4.5\%$, and a total feedback factor ($(\Delta B_{CO}/B_{CO})/(\Delta E_{CO}/(E_{CO} + P_{CO}))$) of 1.19.

O_3 production and export changes are also calculated for each regional reduction to determine whether the transport of O_3 or CO is more important for long-range O_3. Table 7 shows that the change in short-term tropospheric O_3 burden per unit change in CO emissions (Table S9 shows steady-state burden changes) is most sensitive to SE, IN, and AF reductions, which agrees with previous studies showing greater sensitivity of O_3 (especially in the mid- to upper troposphere) to emissions from the tropics, compared to more temperate regions (Fuglestvedt et al., 1999; Berntsen et al., 2005; Naik et al., 2005; West et al., 2009b). In the tropics, stronger photochemistry enhances O_3 and more active convection increases the transport of O_3 and CO to the UT, where O_3 lifetimes are longer (Naik et al., 2005; West et al., 2009b). Table 7 also shows that SE, SA, AF, and IN reductions produce the highest fractions of change in global O_3 production in the UT (above 500 hPa; between 50 and 59%), suggesting that these regions also produce the greatest changes in the vertical convection of CO to the UT. As in West et al. (2009a), the higher water vapor concentrations and convective mixing in the tropics, which would lead to shorter O_3 lifetimes than at higher latitudes (Lawrence et al., 2003), appear to be less important, as CO reductions near the tropics have the greatest influence on global O_3 burden and production.

For all of the regional reductions, more than 70% of the changes in global O_3 burden and global O_3 production occur outside the reduction region, with changes in O_3 production (ΔP) outside the reduction region greatly exceeding changes in O_3 export (ΔX) (Table 7). This demonstrates that the downwind production of O_3 from CO is more important

for long-range O_3 transport than the direct formation and export of O_3 from CO within each source region. This differs from the case of NO_x for which changes in O_3 export exceed changes in O_3 production downwind (West et al., 2009a), reflecting the longer lifetime of CO compared to NO_x.

5 Radiative forcing and global warming potentials

The stratospheric-adjusted net RF impacts for the combined effect of tropospheric O_3, CH_4, and SO_4^{2-} concentration changes are shown in Fig. 8 and Table 8. Annual average net RF distributions show widespread cooling (negative net RFs) across the NH and SH, for all of the regional (and global) CO reductions (Fig. 8), due to global decreases in CH_4 (and long-term O_3) and regional to hemispheric decreases in short-term O_3. Localized to regional cooling and warming patterns, especially from the NA, EU, FSU, and EA reductions, correspond to localized increases and decreases in SO_4^{2-} aerosols (Figs. 7 and 8). While changes in NH_4NO_3 and SOA are not accounted for by the RTM, regional SOA decreases (lesser in magnitude than SO_4^{2-} changes) likely provide slight regional warming, while regional NH_4NO_3 increases and decreases (also less than SO_4^{2-} changes) likely add small regional cooling and warming effects. On the global scale, tropospheric changes in NH_4NO_3 and SOA, like SO_4^{2-}, are expected to contribute little to the global net RF. The large-scale influences of CH_4 and O_3 are consistent with the longwave radiation distributions (Fig. S17), while the local influences of SO_4^{2-} are reflected in the shortwave radiation distributions (Fig. S18). The strongest annual average net RFs occur within the 28° S to 28° N latitudinal band in all cases (Table 8), despite the wide range of reduction regions. This finding is explained by the hotter surface temperatures in the tropics, which result in greater outgoing longwave radiation absorption by greenhouse gases. However, longwave forcings are not as strong directly over the equator, since water vapor is abundant and competes with O_3 absorption in this region (Fig. S17).

Across all 10 regional reductions, the global annual average net RF per unit emissions is -0.12 ± 0.0055 mW m^{-2} (Tg CO yr^{-1})$^{-1}$ (mean ± 1 standard deviation; CV = 0.045), suggesting little variability. Global annual net RF (normalized per unit change in CO emissions), however, is more sensitive to regions close to the equator (ME, SE, and IN). This is consistent with the regions that produce the greatest changes in tropospheric O_3 burden per unit change in CO emissions, but the response for ME emissions is larger than expected given its O_3 burden change (Tables 7, S9), due to the hotter and drier conditions of this region. Monthly global net RF estimates also vary from $\sim 56\%$ less to $\sim 34\%$ greater than the annual mean, with the greatest RFs from June to September (Fig. S20). By doubling the global annual average net RF of the 50% global CO reduction (-0.0361 W m^{-2}) and scaling for biomass burning emissions

Table 7. Changes in global annual average (short-term) tropospheric O_3 burden (B_{O_3}), O_3 production (P_{O_3}), and net O_3 export (X_{O_3}) from each regional reduction, normalized per change in CO emissions (E_{CO}), and the fractions of these above each reduction region and in the upper troposphere (UT). Regional O_3 lifetimes are also shown. For the base simulation, the total global annual average O_3 burden is 352.2 Tg O_3, and the chemical production and loss rates are 4782.5 Tg yr^{-1} and 3975.0 Tg yr^{-1}.

Reduction region	ΔB_{O_3} short-term (Tg O_3)	$\Delta B_{O_3}/$ ΔE_{CO} (days)	ΔP_{O_3} (Tg yr^{-1})	$\Delta P_{O_3}/\Delta E_{CO}$ (Tg O_3) (Tg CO yr$^{-1})^{-1}$)	Regional O_3 lifetime ($\Delta B_{O_3}/\Delta P_{O_3}$) (days)	Fraction of global ΔB_{O_3} above region	Fraction of global ΔP_{O_3} above region	Fraction of global ΔP_{O_3} in UT	ΔX_{O_3} from region (Tg yr^{-1})	ΔP_{O_3} outside region (Tg yr^{-1})
NA	−0.413	4.31	−8.19	−0.234	18.4	0.14	0.30	0.37	−0.91	−5.75
SA	−0.135	4.02	−2.48	−0.202	19.9	0.07	0.17	0.50	−0.12	−2.06
EU	−0.168	3.93	−3.63	−0.233	16.9	0.05	0.18	0.30	−0.34	−2.98
FSU	−0.120	4.00	−2.53	−0.231	17.3	0.13	0.19	0.31	−0.13	−2.06
AF	−0.533	4.48	−9.59	−0.221	20.3	0.12	0.29	0.50	−1.02	−6.83
IN	−0.652	4.94	−11.0	−0.229	21.5	0.04	0.22	0.50	−1.26	−8.67
EA	−0.902	4.31	−16.8	−0.220	19.6	0.06	0.20	0.41	−1.58	−13.4
SE	−0.395	5.31	−6.19	−0.228	23.3	0.05	0.17	0.59	−0.40	−5.15
AU	−0.014	3.49	−0.27	−0.188	18.6	0.05	0.14	0.41	−0.01	−0.24
ME	−0.247	4.23	−4.98	−0.234	18.1	0.08	0.24	0.36	−0.47	−3.78

Table 8. Annual net RF globally and by latitude band (mW m^{-2}) and total GWP$_{20}$ and GWP$_{100}$ estimates for the regional and global reduction simulations relative to the base simulation, due to changes in tropospheric steady-state O_3, CH_4, and SO_4^{2-} concentrations. Global annual net shortwave radiation, net longwave radiation, and net RF per unit change in CO emissions (mW m^{-2} (Tg CO yr$^{-1})^{-1}$) are also shown. The 10 regions estimates represent the sum of the net RFs from all 10 regional reductions; these estimates are not directly estimated by the RTM.

Reduction region	Global annual net RF	Global annual net shortwave radiation	Global annual net longwave radiation	Global annual net RF per Tg CO	Annual net RF 90° S–28° S	Annual net RF 28° S–28° N	Annual net RF 28° N–60° N	Annual net RF 60° N–90° N	Total GWP$_{20}$	Total GWP$_{100}$
NA	−4.25	−0.31	−3.94	−0.122	−2.69	−6.20	−4.76	−3.32	3.98	1.33
SA	−1.51	−0.10	−1.40	−0.123	−1.04	−2.39	−1.45	−0.88	4.04	1.35
EU	−1.79	−0.07	−1.71	−0.114	−1.20	−2.70	−1.72	−1.36	3.71	1.26
FSU	−1.28	−0.07	−1.21	−0.117	−0.85	−1.89	−1.34	−1.00	3.78	1.28
AF	−5.46	−0.55	−4.92	−0.126	−3.61	−8.89	−5.25	−3.11	4.18	1.37
IN	−6.21	−0.85	−5.36	−0.129	−3.60	−10.0	−6.90	−3.70	4.34	1.41
EA	−9.12	−0.61	−8.50	−0.119	−5.80	−13.4	−10.3	−6.71	3.91	1.31
SE	−3.51	−0.34	−3.17	−0.129	−2.21	−5.79	−3.47	−1.99	4.34	1.41
AU	−0.18	−0.004	−0.17	−0.121	−0.12	−0.28	−0.18	−0.11	3.94	1.35
ME	−2.80	−0.40	−2.40	−0.131	−1.68	−4.36	−3.16	−1.81	4.37	1.44
GLOB	−36.1	−3.25	−32.9	−0.124	−22.8	−56.0	−38.6	−24.1	4.07	1.34
10 regions	−36.1	−3.31	−32.8	−0.124	−22.8	−55.9	−38.6	−24.0	–	–

(43.6 % of global anthropogenic CO emissions), which were excluded in the 50 % anthropogenic CO emissions reductions, the global net RF of CO is 0.128 W m^{-2}. This is only ∼11 % greater than the ACCMIP multimodel mean global net RF of CO emissions due to O_3 and CH_4 changes alone (0.115 W m^{-2}; for 1850–2000) (Stevenson et al., 2013). It is smaller than the RF of CO + NMVOC emissions in previous studies: 0.21 ± 0.10 W m^{-2} (Shindell et al., 2005; Forster et al., 2007) and 0.25 ± 0.04 W m^{-2} (Shindell et al., 2009), and is approximately 8.2 % of the global net RF of CO_2 (1.56 W m^{-2}). Among the positive forcing agents with short lifetimes (CO, CH_4, NMVOCs, and BC), our estimated CO RF is ∼8.2 % of their total RF (∼1.57 W m^{-2}) (Forster et al., 2007).

Following the methods of Collins et al. (2013) and Fry et al. (2012), we estimate GWPs for each regional perturbation at 20 and 100 yr time horizons (Table 8, Fig. 9). GWP$_H$ estimates are calculated as the RF integrated to a time horizon H due to an emission pulse, normalized by the change in emissions, and divided by the equivalent for CO_2. Since O_3 RF has both short- and long-term components, we calculate

long-term O_3 RF by scaling the O_3 RF from the CH_4 control simulation by the ratio of long-term O_3 burden changes in each regional perturbation to those of the CH_4 control simulation. We then calculate short-term O_3 RF as the difference between steady-state and long-term O_3 RF. We assume that short-term RF components (SO_4^{2-} and short-term O_3) are constant over one year and then drop to zero instantaneously. Long-term components (CH_4 and long-term O_3) respond and decay with the calculated CH_4 perturbation lifetime (12.48 yr). Figure 9 shows the breakdown of total GWP into short- and long-term components, and error bars representing the average uncertainty of CO GWPs (GWP$_{20}$: ± 1.4 and GWP$_{100}$: ± 0.5) from Fry et al. (2012) across multiple global CTMs (±1 standard deviation). However, the error bars do not account for the full uncertainty, as additional forcings, such as from CO_2, are excluded, which may alter total net RF and GWP estimates. We estimate GWP$_{20}$ and GWP$_{100}$ values of 4.07 and 1.34, respectively, for the global CO reduction, and ranges of 3.71 to 4.37 (CV = 0.059) and 1.26 to 1.44 (CV = 0.043) among regions, suggesting little regional variability.
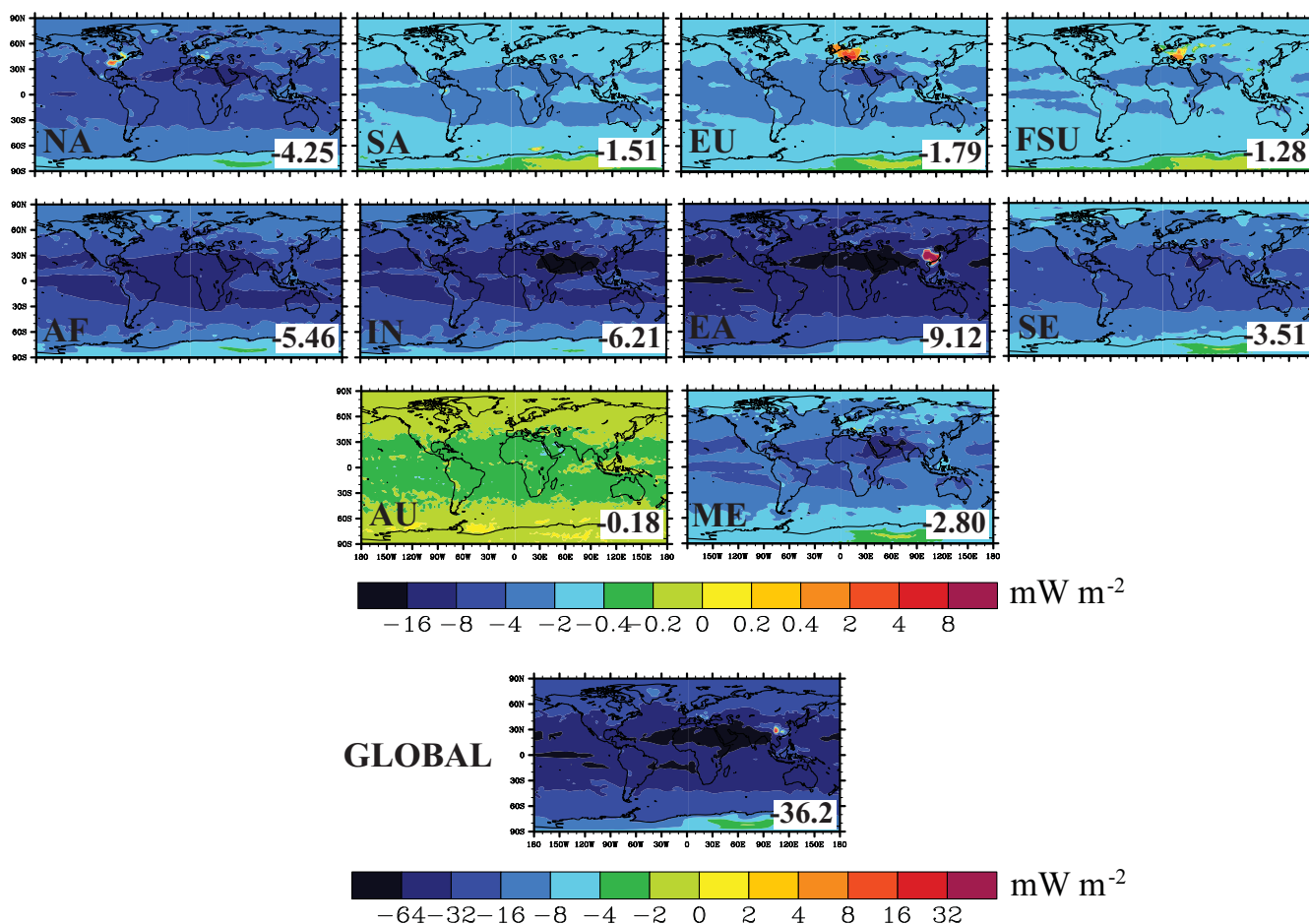
Fig. 8. Annual average net RF distributions (mW m^{-2}) due to changes in tropospheric steady-state O$_3$, CH$_4$, and SO$_4^{2-}$ for the regional and global CO reduction simulations minus the base simulation. Global annual average net RF (mW m^{-2}) for each simulation are noted in the lower right of each panel. Note the difference in scale between the regional and global reductions.

Our GWP$_{100}$ estimates are comparable to those of Derwent et al. (2001) (GWP$_{100}$ of 1.0 due to O$_3$ changes, and 0.6 due to CH$_4$ changes) and Daniel and Solomon (1998) (GWP$_{100}$ of 1.0), yet smaller than the GWP$_{100}$ estimates of Fuglestvedt et al. (1996) (GWP$_{100}$ of 3.0) and Johnson and Derwent (1996) (GWP$_{100}$ of 2.1). Our GWP$_{20}$ and GWP$_{100}$ estimates are also about 65 to 70 % lower than those estimated by Berntsen et al. (2005) for Europe and East Asia, but those did not include SO$_4^{2-}$ impacts as we do here, and 16 to 23 % lower than those estimated by Fry et al. (2012), likely due to differences among the CTMs, such as a lower sensitivity of O$_3$ and CH$_4$ to CO emissions in MOZART-4, but regional definitions also differ (Table S10). Although the absolute GWP estimates of Fry et al. (2012) are more robust than those presented here, reflecting an ensemble of CTMs, the present study more fully addresses the variability of GWPs over a wide range of regions encompassing the tropics and northern and southern extra-tropics.

As mentioned earlier, our GWP estimates do not include the forcing from CO$_2$ once CO oxidizes. This reflects the accounting of carbon emissions in CO$_2$ inventories (Fuglestvedt et al., 1996; Daniel and Solomon, 1998; Collins et al., 2002). If the CO$_2$ forcing were accounted for, the GWP$_{100}$ and GWP$_{20}$ estimates would each increase by 1.57 (44 g CO$_2$ mol^{-1} (28 g CO mol^{-1})$^{-1}$).

6 Conclusions

Reducing CO emissions can slow near-term climate change while improving air quality from O$_3$ and CO itself. The present-day CO RF is estimated as 8.2 % of that from CO$_2$, and also 8.2 % of the short-lived forcing agents that provide an opportunity to slow climate change in the coming decades. We find here that the global net RF of CO reductions varies little among the regions where it is emitted, but CO may cause changes in regional climate that were not quantified. While emission control measures would likely affect
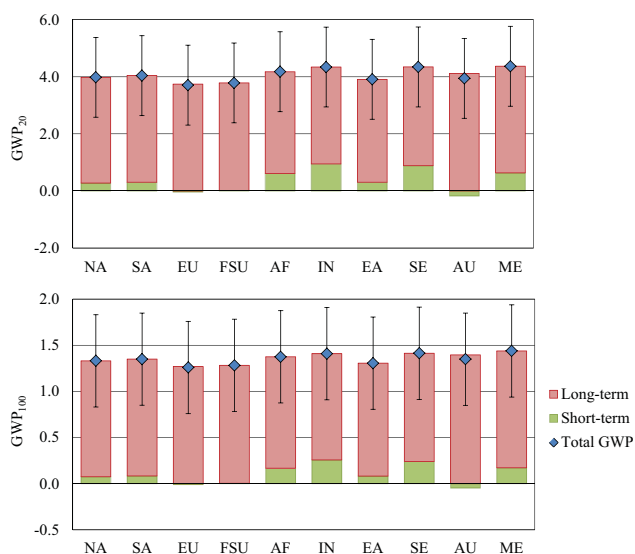
Fig. 9. Global warming potentials for CO at time horizons of 20 and 100 yr (GWP$_{20}$, GWP$_{100}$) for each regional reduction, and the contributions from short-term (O$_3$ and SO$_4^{2-}$ changes) and long-term (long-term O$_3$ and CH$_4$) components. Uncertainty bars represent the average uncertainty found by Fry et al. (2012) based on the spread of atmospheric chemical models (1 standard deviation).

co-emitted species (e.g., BC, OC), this study focuses on the sensitivity of air quality and RF to the location of CO emissions, which is also relevant for determining the GWP of CO. For measures affecting multiple pollutants, the results reported here can be combined with those for co-emitted pollutants.

Halving anthropogenic CO emissions globally and from 10 regions has widespread effects on surface and tropospheric concentrations in addition to net RF. For the global CO emission reduction, global annual net RF, GWP$_{20}$, and GWP$_{100}$ estimates are -0.124 mW m^{-2} (Tg CO)$^{-1}$, 4.07, and 1.34, respectively, with ranges of -0.115 to -0.131 mW m^{-2} (Tg CO)$^{-1}$, 3.71 to 4.37, and 1.26 to 1.44 among the 10 regions, with regions in the tropics (ME, SE, and IN) having the greatest sensitivities. We find little variability in the net RF and GWP estimates among source regions. Our GWP estimates agree well with previous studies (Daniel and Solomon, 1998; Derwent et al., 2001), but are less than the GWP$_{20}$ and GWP$_{100}$ estimates of Berntsen et al. (2005) and Fry et al. (2012), likely related to differences among CTMs. The GWP values should be increased by 1.57 for fossil fuel sources to account for the CO$_2$ generated as an oxidation product. However, care should be taken to avoid double counting, as CO$_2$ emissions are often calculated by assuming complete oxidation of the fuel rather than being measured in the exhaust. It is always preferable for climate to emit the carbon as CO$_2$ rather than CO.

Net RF distributions for the regional (and global) reductions show widespread cooling across the NH and SH corresponding to the patterns of regional short-term O$_3$ and global CH$_4$ (and long-term O$_3$) decreases, and localized positive and negative net RFs due to changes in SO$_4^{2-}$ aerosols. The strongest annual net RFs occur within the tropics (28° S to 28° N), independent of the location of CO emissions change, due to higher temperatures and greater absorption of infrared radiation.

For all regional reductions, we show that the greatest changes in surface CO and O$_3$ concentrations are within the reduction region, with lesser decreases hemispherically. The regions with the highest anthropogenic CO emissions (EA, IN, AF, and NA) show the largest impacts on surface CO and O$_3$ concentrations within that region and between regions. The impact of EA's reduction on US surface CO and O$_3$ concentrations is 39 and 93 %, respectively, of that resulting from NA. The NA CO reduction also has a strong impact on EU and ME surface O$_3$ concentrations. Anthropogenic CO emissions overall contribute ∼6.1 % (1.6 ppbv) to global annual average steady-state surface O$_3$, by doubling the change from the 50 % global CO reduction (-0.45 ppbv) and scaling for biomass burning emissions.

All of the reductions increase tropospheric OH leading to decreases in global CH$_4$ and hence, long-term O$_3$. At the same time, tropospheric H$_2$O$_2$ decreases in all cases. We generally find that increases in OH contribute to increases in SO$_4^{2-}$ through gas-phase oxidation, which is dominant in drier regions and near the equator. Decreases in H$_2$O$_2$ and O$_3$ contribute to decreases in SO$_4^{2-}$ via aqueous-phase oxidation, which prevails mostly in the northern midlatitudes.

For all regional reductions, more than 70 % of the global O$_3$ burden and production changes, and more than 79 % of global CO burden changes, occur outside the reduction region. In addition, O$_3$ production changes outside the source region greatly exceed changes in O$_3$ export from each region, suggesting that long-range O$_3$ is influenced substantially by the transport of CO and subsequent production of O$_3$ downwind, and less by the transport of O$_3$ itself. Tropospheric O$_3$ burden changes (per unit change in CO emissions) are most sensitive to SE, IN, and AF reductions, due to stronger photochemistry and more active vertical convection in the tropics compared to other regions (Naik et al., 2005; West et al., 2009a).

Limitations of this study include only accounting for O$_3$, CH$_4$, and SO$_4^{2-}$ changes in net RF and GWP estimates. We exclude changes in nitrate aerosols, secondary organic aerosols, stratospheric O$_3$, water vapor, the carbon cycle via O$_3$ and nitrogen deposition, and CO$_2$, as these components are not part of the current RTM configuration. Our RTM simulations also do not include the indirect effects of aerosols on clouds or the internal mixing of aerosols, but these effects may be large. We estimate only small changes in NH$_4$NO$_3$ and SOA, consistent with previous studies that show these aerosols contributing much less to CO RF than

SO_4^{2-} (Shindell et al., 2009). Stratospheric O_3 and water vapor RFs are believed to be relatively small (Forster et al., 2007). The contribution of CO emissions to CO_2 RF via changes in the CO_2 uptake by plants is estimated as 12 and 42 % of the net RF (Fry et al., 2012), which would increase GWPs and perhaps the variability among regions, depending on regional vegetation distributions.

We do not assess climate responses as in Shindell and Faluvegi (2009), but show how CO emissions location affects the latitudinal distribution of net RF and CO GWPs. Regional CO emissions are also considered fairly uncertain (Duncan et al., 2007), according to a number of studies that have used inverse modeling or adjoint methods to constrain CO emissions by satellite data (Heald et al., 2004; Pétron et al., 2004; Pfister et al., 2004, 2005; Kopacz et al., 2009, 2010), but this uncertainty likely does not strongly influence normalized forcings and GWPs. Uncertainties in the emissions of other O_3 precursors and in MOZART-4's chemical and transport processes are likewise important (Berntsen et al., 2005). Future work could examine the influence of dynamic climate feedbacks on chemistry, and future changes in emissions that may alter the air quality and RF sensitivities given here for present-day emissions.

Future international climate agreements or emissions trading mechanisms could include CO among a suite of long-lived greenhouse gases, using a single GWP globally, given that the uncertainty in the global GWP for CO is greater than the range among regions estimated here. Alternatively, different GWPs could be applied to different continents. In either case, this work provides an incentive to reduce CO emissions, as part of coordinated policies addressing climate and air quality.

Supplementary material related to this article is available online at: http://www.atmos-chem-phys.net/13/5381/2013/acp-13-5381-2013-supplement.pdf.

References

Akimoto, H.: Global air quality and pollution, Science, 302, 1716–1719, doi:10.1126/science.1092666, 2003.

Barth, M. C., Rasch, P. J., Kiehl, J. T., Benkovitz, C. M., and Schwartz, S. E.: Sulfur chemistry in the National Center for Atmospheric Research Community Climate Model: Description, evaluation, features, and sensitivity to aqueous chemistry, J. Geophys. Res., 105, 1387–1415, 2000.

Bauer, S. E., Koch, D., Unger, N., Metzger, S. M., Shindell, D. T., and Streets, D. G.: Nitrate aerosols today and in 2030: a global simulation including aerosols and tropospheric ozone, Atmos. Chem. Phys., 7, 5043–5059, doi:10.5194/acp-7-5043-2007, 2007.

Berntsen, T. K., Fuglestvedt, J. S., Joshi, M. M., Shine, K. P., Stuber, N., Ponater, M., Sausen, R., Hauglustaine, D. A., and Li, L.: Response of climate to regional emissions of ozone precursors: sensitivities and warming potentials, Tellus, 57B, 283–304, doi:10.1111/j.1600-0889.2005.00152.x, 2005.

Chung, S. and Seinfeld, J.: Global distribution and climate forcing of carbonaceous aerosols, J. Geophys. Res., 107, 4407, doi:10.1029/2001JD001397, 2002.

Cionni, I., Eyring, V., Lamarque, J.-F., Randel, W. J., Stevenson, D. S., Wu, F., Bodeker, G. E., Shepherd, T. G., Shindell, D. T., and Waugh, D. W.: Ozone database in support of CMIP5 simulations: results and corresponding radiative forcing, Atmos. Chem. Phys., 11, 11267–11292, doi:10.5194/acp-11-11267-2011, 2011.

Collins, W. J., Derwent, R. G., Johnson, C. E., and Stevenson, D. S.: The oxidation of organic compounds in the troposphere and their global warming potentials, Climatic Change, 52, 453–479, doi:10.1023/A:1014221225434, 2002.

Collins, W. J., Fry, M. M., Yu, H., Fuglestvedt, J. S., Shindell, D. T., and West, J. J.: Global and regional temperature-change potentials for near-term climate forcers, Atmos. Chem. Phys., 13, 2471–2485, doi:10.5194/acp-13-2471-2013, 2013.

Daniel, J. S. and Solomon, S.: On the climate forcing of carbon monoxide, J. Geophys. Res., 103, 13249–13260, doi:10.1029/98JD00822, 1998.

Derwent, R. G., Collins, W. J., Johnson, C. E., and Stevenson, D. S.: Transient behaviour of tropospheric ozone precursors in a global 3-D CTM and their indirect greenhouse effects, Climatic Change, 49, 463–487, doi:10.1023/A:1010648913655, 2001.

Duncan, B. N., Logan, J. A., Bey, I., Megretskaia, I. A., Yantosca, R. M., Novelli, P. C., Jones, N. B., and Rinsland, C. P.: The global budget of CO, 1988–1997: Source estimates and validation with a global model, J. Geophys. Res., 112, D22301, doi:10.1029/2007JD008459, 2007.

Emmons, L. K., Walters, S., Hess, P. G., Lamarque, J.-F., Pfister, G. G., Fillmore, D., Granier, C., Guenther, A., Kinnison, D., Laepple, T., Orlando, J., Tie, X., Tyndall, G., Wiedinmyer, C., Baughcum, S. L., and Kloster, S.: Description and evaluation of the Model for Ozone and Related chemical Tracers, version 4 (MOZART-4), Geosci. Model Dev., 3, 43–67, doi:10.5194/gmd-3-43-2010, 2010.

Fiore, A. M., Jacob, D. J., Field, B. D., Streets, D. G., Fernandes, S. D., and Jang, C.: Linking ozone pollution and climate change: The case for controlling methane, Geophys. Res. Lett., 29, 1919, doi:10.1029/2002GL015601, 2002.

Fiore, A. M., West, J. J., Horowitz, L. W., Naik, V., and Schwarzkopf, M. D.: Characterizing the tropospheric ozone

response to methane emission controls and the benefits to climate and air quality, J. Geophys. Res., 113, D08307, doi:10.1029/2007JD009162, 2008.

Fiore, A. M., Dentener, F. J., Wild, O., Cuvelier, C., Schultz, M. G., Hess, P., Textor, C., Schulz, M., Doherty, R. M., Horowitz, L. W., MacKenzie, I. A., Sanderson, M. G., Shindell, D. T., Stevenson, D. S., Szopa, S., Van Dingenen, R., Zeng, G., Atherton, C., Bergmann, D., Bey, I., Carmichael, G., Collins, W. J., Duncan, B. N., Faluvegi, G., Folberth, G., Gauss, M., Gong, S., Hauglustaine, D., Holloway, T., Isaksen, I. S. A., Jacob, D. J., Jonson, J. E., Kaminski, J. W., Keating, T. J., Lupu, A., Marmer, E., Montanaro, V., Park, R. J., Pitari, G., Pringle, K. J., Pyle, J. A., Schroeder, S., Vivanco, M. G., Wind, P., Wojcik, G., Wu, S., and Zuber, A.: Multimodel estimates of intercontinental source-receptor relationships for ozone pollution, J. Geophys. Res., 114, D04301, doi:10.1029/2008JD010816, 2009.

Forster, P., Ramaswamy, V., Artaxo, P., Berntsen, T., Betts, R., Fahey, D. W., Haywood, J., Lean, J., Lowe, D. C., Myhre, G., Nganga, J., Prinn, R., Raga, G., Schulz, M., and Van Dorland, R.: Changes in atmospheric constituents and in radiative forcing, in: Climate Change 2007: The Physical Science Basis. Contribution of Working Group I to the Fourth Assessment Report of the Intergovernmental Panel on Climate Change, edited by: Solomon, S., Qin, D., Manning, M., Chen, Z., Marquis, M., Averyt, K. B., Tignor, M., and Miller, H. L., Cambridge Univ. Press, Cambridge, UK, 129–234, 2007.

Forster, P. M. D. and Shine, K. P.: Radiative forcing and temperature trends from stratospheric ozone changes, J. Geophys. Res., 102, 10481–10857, doi:10.1029/96JD03510, 1997.

Fry, M. M., Naik, V., West, J. J., Schwarzkopf, M. D., Fiore, A. M., Collins, W. J., Dentener, F. J., Shindell, D. T., Atherton, C., Bergmann, D., Duncan, B. N., Hess, P., MacKenzie, I. A., Marmer, E., Schultz, M. G., Szopa, S., Wild, O., and Zeng, G.: The influence of ozone precursor emissions from four world regions on tropospheric composition and radiative climate forcing, J. Geophys. Res., 117, D07306, doi:10.1029/2011JD017134, 2012.

Fuglestvedt, J. S., Isaksen, I. S. A., and Wang, W.-C.: Estimates of indirect global warming potentials for CH_4, CO, and NO_x. Clim. Change, 34, 405–437, 1996.

Fuglestvedt, J. S., Berntsen, T. K., Isaksen, I. S. A., Mao, H. T., Liang, X. Z., and Wang, W. C.: Climatic forcing of nitrogen oxides through changes in tropospheric ozone and methane; global 3D model studies, Atmos. Environ., 33, 961–977, doi:10.1016/S1352-2310(98)00217-9, 1999.

GFDL Global Atmospheric Model Development Team (GAMDT): The new GFDL global atmosphere and land model AM2-LM2: Evaluation with prescribed SST simulations, J. Clim., 17, 4641–4673, 2004.

Granier, C., Guenther, A., Lamarque, J., Mieville, A., Muller, J., Olivier, J., Orlando, J., Peters, J., Petron, G., Tyndall, G., and Wallens, S.: POET, a database of surface emissions of ozone precursors, available at: http://accent.aero.jussieu.fr/POET_metadata.php, 2005.

Guenther, A., Karl, T., Harley, P., Wiedinmyer, C., Palmer, P. I., and Geron, C.: Estimates of global terrestrial isoprene emissions using MEGAN (Model of Emissions of Gases and Aerosols from Nature), Atmos. Chem. Phys., 6, 3181-3210, doi:10.5194/acp-6-3181-2006, 2006.

Heald, C. L., Jacob, D. J., Fiore, A. M., Emmons, L. K., Gille, J. C., Deeter, M. N., Warner, J., Edwards, D. P., Crawford, J. H., Hamlin, A. J., Sachse, G. W., Browell, E. V., Avery, M. A., Vay, S. A., Westberg, D. J., Blake, D. R., Singh, H. B., Sandholm, S. T., Talbot, R. W., and Fuelberg, H. E.: Asian outflow and trans-Pacific transport of carbon monoxide and ozone pollution: An integrated satellite, aircraft and model perspective, J. Geophys. Res., 108, 4804, doi:10.1029/2003JD003507, 2003.

Heald, C. L., Jacob, D. J., Jones, D. B. A., Palmer, P. I., Logan, J. A., Streets, D. G., Sachse, G. W., Gille, J. C., Hoffman, R. N., and Nehrkorn, T.: Comparative inverse analysis of satellite (MO-PITT) and aircraft (TRACE-P) observations to estimate Asian sources of carbon monoxide, J. Geophys. Res., 109, D15S04, doi:10.1029/2004JD005185, 2004.

Horowitz, L. W., Fiore, A. M., Milly, G. P., Cohen, R. C., Perring, A., Wooldridge, P. J., Hess, P. G., Emmons, L. K., and Lamarque, J.-F.: Observational constraints on the chemistry of isoprene nitrates over the eastern United States, J. Geophys. Res, 112, D12S08, doi:10.1029/2006JD007747, 2007.

Hoyle, C. R., Myhre, G., Berntsen, T. K., and Isaksen, I. S. A.: Anthropogenic influence on SOA and the resulting radiative forcing, Atmos. Chem. Phys., 9, 2715–2728, doi:10.5194/acp-9-2715-2009, 2009.

Hudman, R. C., Moore, N. E., Mebust, A. K., Martin, R. V., Russell, A. R., Valin, L. C., and Cohen, R. C.: Steps towards a mechanistic model of global soil nitric oxide emissions: implementation and space based-constraints, Atmos. Chem. Phys., 12, 7779–7795, doi:10.5194/acp-12-7779-2012, 2012.

Jackson, S. C.: Parallel Pursuit of Near-term and Long-term Climate Mitigation, Science, 326, 526–527, doi:10.1126/science.1177042, 2009.

Jacob, D. J.: Introduction to Atmospheric Chemistry, Princeton University Press, Princeton, NJ, USA, 52–53, 1999.

Johnson, C. E. and Derwent, R. G.: Relative radiative forcing consequences of global emissions of hydrocarbons, carbon monoxide, and NO_x from human activities estimated with a zonally-averaged two-dimensional model. Clim. Change, 34, 439–462, 1996.

Kopacz, M., Jacob, D. J., Henze, D. K., Heald, C. L., Streets, D. G., and Zhang, Q.: Comparison of adjoint and analytical Bayesian inversion methods for constraining Asian sources of carbon monoxide using satellite (MOPITT) measurements of CO columns, J. Geophys. Res., 114, D04305, doi:10.1029/2007JD009264, 2009.

Kopacz, M., Jacob, D. J., Fisher, J. A., Logan, J. A., Zhang, L., Megretskaia, I. A., Yantosca, R. M., Singh, K., Henze, D. K., Burrows, J. P., Buchwitz, M., Khlystova, I., McMillan, W. W., Gille, J. C., Edwards, D. P., Eldering, A., Thouret, V., and Nedelec, P.: Global estimates of CO sources with high resolution by adjoint inversion of multiple satellite datasets (MOPITT, AIRS, SCIAMACHY, TES), Atmos. Chem. Phys., 10, 855–876, doi:10.5194/acp-10-855-2010, 2010.

Lacis, A. A., Wuebbles, D. J., and Logan, J. A.: Radiative forcing of climate by changes in the vertical distribution of ozone, J. Geophys. Res., 95, 9971–9981, doi:10.1029/JD095iD07p09971, 1990.

Lamarque, J.-F., Kiehl, J. T., Hess, P. G., Collins, W. D., Emmons, L. K., Ginoux, P., Luo, C., and Tie, X. X.: Response of a coupled chemistry-climate model to changes in aerosol emis-

sions: Global impact on the hydrological cycle and the tropospheric burdens of OH, ozone, and NOx, Geophys. Res. Lett., 32, L16809, doi:10.1029/2005GL023419, 2005.

Lapina, K., Honrath, R. E., Owen, R. C., Martin, M. V., and Pfister, G.: Evidence of significant large-scale impacts of boreal fires on ozone levels in the midlatitude Northern Hemisphere free troposphere, Geophys. Res. Lett., 33, L10815, doi:10.1029/2006GL025878, 2006.

Lawrence, M. G.: Photochemistry in the tropical pacific troposphere: Studies with a global 3D chemistry-meteorology model, Ph.D. thesis, Georgia Institute of Technology, Georgia, USA, 1996.

Lawrence, M. G., Crutzen, P. J., Rasch, P. J., Eaton, B. E., and Mahowald, N. M.: A model for studies of tropospheric photochemistry: Description, global distributions, and evaluation, J. Geophys. Res., 104, 26245–26277, 1999.

Lawrence, M. G., von Kuhlmann, R., Salzmann, M., and Rasch, P. J.: The balance of effects of deep convective mixing on tropospheric ozone, Geophys. Res. Lett., 30, 1940, doi:10.1029/2003GL017644, 2003.

Leibensperger, E. M., Mickley, L. J., Jacob, D. J., and Barrett, S. R. H.: Intercontinental influence of NO_X and CO emissions on particulate matter air quality, Atmos. Environ., 45, 3318–3324, doi:10.1016/j.atmosenv.2011.02.023, 2011.

Meinshausen, M., Smith, S. J., Calvin, K. V., Daniel, J. S., Kainuma, M. L. T., Lamarque, J.-F., Matsumoto, K., Montzka, S. A., Raper, S. C. B., Riahi, K., Thomson, A. M., Velders, G. J. M., and van Vuuren, D.: The RCP Greenhouse Gas Concentrations and their Extension from 1765 to 2300, Climatic Change (Special Issue), 109, 213–241, doi:10.1007/s10584-011-0156-z, 2011.

Metzger, S., Dentener, F., Pandis, S., and Lelieveld, J.: Gas/aerosol partitioning: 1. A computationally efficient model, J. Geophys. Res., 107, 4312, doi:10.1029/2001JD001102, 2002.

Naik, V., Mauzerall, D., Horowitz, L., Schwarzkopf, M. D., Ramaswamy, V., and Oppenheimer, M.: Net radiative forcing due to changes in regional emissions of tropospheric ozone precursors, J. Geophys. Res., 110, D24306, doi:10.1029/2005JD005908, 2005.

Naik, V., Mauzerall, D. L., Horowitz, L. W., Schwarzkopf, M. D., Ramaswamy, V., and Oppenheimer, M.: On the sensitivity of radiative forcing from biomass burning aerosols and ozone to emission location, Geophys. Res. Lett., 34, L03818, doi:10.1029/2006GL028149, 2007.

Olivier, J., Peters, J., Granier, C., Petron, G., Muller, J., and Wallens, S.: Present and future surface emissions of atmospheric compounds, POET report #2, EU project EVK2-1999-00011, available at: http://accent.aero.jussieu.fr/POET_metadata.php, 2003.

Pétron, G., Granier, C., Khattatov, B., Yudin, V., Lamarque, J., Emmons, L., Gille, J., and Edwards, D. P.: Monthly CO surface sources inventory based on the 2000–2001 MOPITT satellite data, Geophys. Res. Lett., 31, L21107, doi:10.1029/2004GL020560, 2004.

Pfister, G., Pétron, G., Emmons, L. K., Gille, J. C., Edwards, D. P., Lamarque, J.-F., Attié, J.-L., Granier, C., and Novelli, P. C.: Evaluation of CO simulations and the analysis of the CO budget for Europe, J. Geophys. Res., 109, D19304, doi:10.1029/2004JD004691, 2004.

Pfister, G., Hess, P., Emmons, L., Lamarque, J.-F., Wiedinmeyer, C., Edwards, D., Pétron, G., Gille, J., and Sachse, G.: Quantifying CO emissions from the 2004 Alaskan wildfires using MOPITT CO data, Geophys. Res. Lett., 32, L11809, doi:10.29/2005GL022995, 2005.

Pfister, G. G., Emmons, L. K., Hess, P. G., Honrath, R., Lamarque, J.-F., Val Martin, M., Owen, R. C., Avery, M. A., Browell, E. V., Holloway, J. S., Nedelec, P., Purvis, R., Ryerson, T. B., Sachse, G. W., and Schlager, H.: Ozone production from the 2004 North American boreal fires, J. Geophys. Res., 111, D24S07, doi:10.1029/2006JD007695, 2006.

Pfister, G. G., Emmons, L. K., Hess, P. G., Lamarque, J.-F., Orlando, J. J., Walters, S., Guenther, A., Palmer, P. I., and Lawrence, P. J.: Contribution of isoprene to chemical budgets: A model tracer study with the NCAR CTM MOZART-4, J. Geophys. Res., 113, D05308, doi:10.1029/2007JD008948, 2008.

Pham, M., Muller, J. F., Brasseur, G. P., Granier, C. and Megie, G.: A three-dimensional study of the tropospheric sulfur cycle, J. Geophys. Res., 100, 26061–26092, doi:10.1029/95JD02095, 1995.

Prather, M. J.: Time scales in atmospheric chemistry: Theory, GWPs for CH_4 and CO, and runaway growth, Geophys. Res. Lett., 23, 2597–2600, doi:10.1029/96GL02371, 1996.

Prather, M., Ehhalt, D., Dentener, F., Derwent, R. G., Dlugokencky, E., Holland, E., Isaksen, I. S. A., Katima, J., Kirchhoff, V., Matson, P., Midgley, P. M., and Wang, M.: Climate Change 2001: The Scientific Basis, Atmospheric Chemistry and Greenhouse Gases, Chap. 4, Cambridge Univ. Press, New York, USA, 239–287, 2001.

Prather, M. J., Holmes, C. D., and Hsu, J. J.: Reactive greenhouse gas scenarios: systematic exploration of uncertainties and the role of atmospheric chemistry, Geophys. Res. Lett., 39, L09803, doi:10.1029/2012GL051440, 2012.

Riahi, K., Gruebler, A., and Nakicenovic, N.: Scenarios of long-term socio-economic and environmental development under climate stabilization, Technol. Forecast. Soc. Change, 74, 7, 887–935, 2007.

Riahi, K., Rao, S., Krey, V., Cho, C., Chirkov, V., Fischer, G., Kindermann, G., Nakicenovic, N., and Rafaj, P.: RCP 8.5 – A scenario of comparatively high greenhouse gas emissions, Climatic Change, 109, 33–57, doi:10.1007/s10584-011-0149-y, 2011.

Rienecker, M. M., Suarez, M. J., Todling, R., Bacmeister, J., Takacs, L., Liu, H.-C., Gu, W., Sienkiewicz, M., Koster, R. D., Gelaro, R., Stajner, I., and Nielsen, J. E.: The GEOS-5 Data Assimilation System – Documentation of versions 5.0.1, 5.1.0, and 5.2.0, NASA Tech. Memo., NASA/TM-2008-104606, 27, 118 pp., 2008.

Rypdal, K., Berntsen, T., Fuglestvedt, J. S., Aunan, K., Torvanger, A., Stordal, F., Pacyna, J. M., and Nygaard, L. P.: Tropospheric ozone and aerosols in climate agreements: scientific and political challenges, Environ. Sci. Pol., 8, 29–43, doi:10.1016/j.envsci.2004.09.003, 2005.

Rypdal, K., Rive, N., Berntsen, T., Fagerli, H., Klimont, Z., Mideksa, T. K., and Fuglestvedt, J. S.: Climate and air quality-driven scenarios of ozone and aerosol precursor abatement, Environ. Sci. Pol., 12, 7, 855–869, doi:10.1016/j.envsci.2009.08.002, 2009.

Saikawa, E., Naik, V., Horowitz, L. W., Liu, J. F., and Mauzerall, D. L.: Present and potential future contributions of sulfate, black and organic carbon aerosols from China to global air quality, premature mortality and radiative forcing, Atmos. Environ., 43, 2814–

2822, doi:10.1016/j.atmosenv.2009.02.017, 2009.

Schultz, M. G., Backman, L., Balkanski, Y., Bjoerndalsaeter, S., Brand, R., Burrows, J. P., Dalsoeren, S., de Vasconcelos, M., Grodtmann, B., Hauglustaine, D. A., Heil, A., Hoelzemann, J. J., Isaksen, I. S. A., Kaurola, J., Knorr, W., Ladstaetter-Weißenmayer, A., Mota, B., Oom, D., Pacyna, J., Panasiuk, D., Pereira, J. M. C., Pulles, T., Pyle, J., Rast, S., Richter, A., Savage, N., Schnadt, C., Schulz, M., Spessa, A., Staehelin, J., Sundet, J. K., Szopa, S., Thonicke, K., van het Bolscher, M., van Noije, T., van Velthoven, P., Vik, A. F., and Wittrock, F.: REanalysis of the TROpospheric chemical composition over the past 40 years (RETRO) – A long-term global modeling study of tropospheric chemistry, Final Report, Jülich/Hamburg, Germany, 2007.

Schumann, U. and Huntrieser, H.: The global lightning-induced nitrogen oxides source, Atmos. Chem. Phys., 7, 3823–3907, doi:10.5194/acp-7-3823-2007, 2007.

Schwarzkopf, M. D. and Ramaswamy, V.: Radiative effects of CH_4, N_2O, halocarbons and the foreign-broadened H_2O continuum: A GCM experiment, J. Geophys. Res., 104, 9467–9488, doi:10.1029/1999JD900003, 1999.

Shindell, D. and Faluvegi, G.: Climate response to regional radiative forcing during the twentieth century, Nature Geosci., 2, 294–300, doi:10.1038/NGEO473, 2009.

Shindell, D. T., Faluvegi, G., Bell, N., and Schmidt, G. A.: An emissions-based view of climate forcing by methane and tropospheric ozone, Geophys. Res. Lett., 32, L04803, doi:10.1029/2004GL021900, 2005.

Shindell, D. T., Faluvegi, G., Stevenson, D. S., Krol, M. C., Emmons, L. K., Lamarque, J.-F., Pétron, G., Dentener, F. J., Ellingsen, K., Schultz, M. G., Wild, O., Amann, M., Atherton, C. S., Bergmann, D. J., Bey, I., Butler, T., Cofala, J., Collins, W. J., Derwent, R. G., Doherty, R. M., Drevet, J., Eskes, H. J., Fiore, A. M., Gauss, M., Hauglustaine, D. A., Horowitz, L. W., Isaksen, I. S. A., Lawrence, M. G., Montanaro, V., Müller, J.-F., Pitari, G., Prather, M. J., Pyle, J. A., Rast, S., Rodriguez, J. M., Sanderson, M. G., Savage, N. H., Strahan, S. E., Sudo, K., Szopa, S., Unger, N., van Noije, T. P. C., and Zeng, G.: Multimodel simulations of carbon monoxide: Comparison with observations and projected near-future changes, J. Geophys. Res., 111, D19306, doi:10.1029/2006JD007100, 2006.

Shindell, D. T., Faluvegi, G., Koch, D. M., Schmidt, G. A., Unger, N., and Bauer, S. E.: Improved attribution of climate forcing to emissions, Science, 326, 716–718, doi:10.1126/science.1174760, 2009.

Shindell, D., Kuylenstierna, J. C. I., Vignati, E., van Dingenen, R., Amann, M., Klimont, Z., Anenberg, S. C., Muller, N., Janssens-Maenhout, G., Raes, F., Schwartz, J., Faluvegi, G., Pozzoli, L., Kupiainen, K., Höglund-Isaksson, L., Emberson, L., Streets, D., Ramanathan, V., Hicks, K., Oanh, N. T. K., Milly, G., Williams, M., Demkine, V., and Fowler, D.: Simultaneously mitigating near-term climate change and improving human health and food security, Science, 335, 183–189, doi:10.1126/science.1210026, 2012.

Søvde, O. A., Hoyle, C. R., Myhre, G., and Isaksen, I. S. A.: The HNO_3 forming branch of the $HO_2 + NO$ reaction: pre-industrial-to-present trends in atmospheric species and radiative forcings, Atmos. Chem. Phys., 11, 8929–8943, doi:10.5194/acp-11-8929-2011, 2011.

Spivakovsky, C. M., Logan, J. A., Montzka, S. A., Balkanski, Y. J., Foreman-Fowler, M., Jones, D. B. A., Horowitz, L. W., Fusco, A. C., Brenninkmeijer, C. A. M., Prather, M. J., Wofsy, S. C., and McElroy, M. B.: Three-dimensional climatological distribution of tropospheric OH: Update and evaluation, J. Geophys. Res., 105, 8931–8980, 2000.

Stevenson, D. S., Dentener, F. J., Schultz, M. G., Ellingsen, K., van Noije, T. P. C., Wild, O., Zeng, G., Amann, M., Atherton, C. S., Bell, N., Bergmann, D. J., Bey, I., Butler, T., Cofala, J., Collins, W. J., Derwent, R. G., Doherty, R. M., Drevet, J., Eskes, H. J., Fiore, A. M., Gauss, M., Hauglustaine, D. A., Horowitz, L. W., Isaksen, I. S. A., Krol, M. C., Lamarque, J.-F., Lawrence, M. G., Montanaro, V., Müller, J.-F., Pitari, G., Prather, M. J., Pyle, J. A., Rast, S., Rodriguez, J. M., Sanderson, M. G., Savage, N. H., Shindell, D. T., Strahan, S. E., Sudo, K., and Szopa, S.: Multimodel ensemble simulations of present-day and near-future tropospheric ozone, J. Geophys. Res., 111, D08301, doi:10.1029/2005JD006338, 2006.

Stevenson, D. S., Young, P. J., Naik, V., Lamarque, J.-F., Shindell, D. T., Voulgarakis, A., Skeie, R. B., Dalsoren, S. B., Myhre, G., Berntsen, T. K., Folberth, G. A., Rumbold, S. T., Collins, W. J., MacKenzie, I. A., Doherty, R. M., Zeng, G., van Noije, T. P. C., Strunk, A., Bergmann, D., Cameron-Smith, P., Plummer, D. A., Strode, S. A., Horowitz, L., Lee, Y. H., Szopa, S., Sudo, K., Nagashima, T., Josse, B., Cionni, I., Righi, M., Eyring, V., Conley, A., Bowman, K. W., Wild, O., and Archibald, A.: Tropospheric ozone changes, radiative forcing and attribution to emissions in the Atmospheric Chemistry and Climate Model Intercomparison Project (ACCMIP), Atmos. Chem. Phys., 13, 3063–3085, doi:10.5194/acp-13-3063-2013, 2013.

Task Force on Hemispheric Transport of Air Pollution (TF HTAP): Hemispheric Transport of Air Pollution, United Nations Economic Commission for Europe, Geneva, Switzerland, 2010.

Tilmes, S., Lamarque, J.-F., Emmons, L. K., Conley, A., Schultz, M. G., Saunois, M., Thouret, V., Thompson, A. M., Oltmans, S. J., Johnson, B., and Tarasick, D.: Technical Note: Ozonesonde climatology between 1995 and 2011: description, evaluation and applications, Atmos. Chem. Phys., 12, 7475–7497, doi:10.5194/acp-12-7475-2012, 2012.

Unger, N., Shindell, D. T., Koch, D. M., and Streets, D. G.: Cross influences of ozone and sulfate precursor emissions changes on air quality and climate, Proc. Natl. Acad. Sci., 103, 12, 4377–4380, doi:10.1073/pnas.0508769103, 2006.

von Kuhlmann, R.: Photochemistry of tropospheric ozone, its precursors and the hydroxyl radical: A 3D-modeling study considering non-methane hydrocarbons, Ph.D. thesis, Johannes Gutenberg-Universität Mainz, Mainz, Germany, 2001.

Voulgarakis, A., Naik, V., Lamarque, J.-F., Shindell, D. T., Young, P. J., Prather, M. J., Wild, O., Field, R. D., Bergmann, D., Cameron-Smith, P., Cionni, I., Collins, W. J., Dalsøren, S. B., Doherty, R. M., Eyring, V., Faluvegi, G., Folberth, G. A., Horowitz, L. W., Josse, B., MacKenzie, I. A., Nagashima, T., Plummer, D. A., Righi, M., Rumbold, S. T., Stevenson, D. S., Strode, S. A., Sudo, K., Szopa, S., and Zeng, G.: Analysis of present day and future OH and methane lifetime in the ACCMIP simulations, Atmos. Chem. Phys., 13, 2563–2587, doi:10.5194/acp-13-2563-2013, 2013.

Wang, W. C., Zhuang, Y. C., and Bojkov, R. D.: Climatic implications of observed changes in ozone vertical distribution in the

middle and high latitudes of the Northern Hemisphere, Geophys. Res. Lett., 20, 1567–1570, doi:10.1029/93GL01318, 1993.

West, J. J., Fiore, A. M., Naik, V., Horowitz, L. W., Schwarzkopf, M. D., and Mauzerall, D. L.: Ozone air quality and radiative forcing consequences of changes in ozone precursor emissions, Geophys. Res. Lett., 34, L06806, doi:10.1029/2006GL029173, 2007.

West, J. J., Naik, V., Horowitz, L. W., and Fiore, A. M.: Effect of regional precursor emission controls on long-range ozone transport – Part 1: Short-term changes in ozone air quality, Atmos. Chem. Phys., 9, 6077–6093, doi:10.5194/acp-9-6077-2009, 2009a.

West, J. J., Naik, V., Horowitz, L. W., and Fiore, A. M.: Effect of regional precursor emission controls on long-range ozone transport – Part 2: Steady-state changes in ozone air quality and impacts on human mortality, Atmos. Chem. Phys., 9, 6095–6107, doi:10.5194/acp-9-6095-2009, 2009b.

Wild, O., Prather, M. J., and Akimoto, H.: Indirect long-term global radiative cooling from NO_x emissions, Geophys. Res. Lett., 28, 1719–1722, doi:10.1029/2000GL012573, 2001.

World Meteorological Organization (WMO): WMO Greenhouse Gas Bulletin: The State of Greenhouse Gases in the Atmosphere using Global Observations through 2005, Bulletin No. 1, March 2006, 2006.